AD-A196 477

UNCLASSIFIED

SECURITY CLASSIFICATION OF THIS PAGE (When Data Entered)

DTIC FILE COPY

1

REPORT DOCUMENTATION PAGE

READ INSTRUCTIONS BEFORE COMPLETING FORM

1. REPORT NUMBER: AFIT/CI/NR 88- 157	2. GOVT ACCESSION NO.
3. RECIPIENT'S CATALOG NUMBER	
4. TITLE (and Subtitle): SIZE EFFECTS IN LINEAR ELASTIC FRACTURE MECHANICS	5. TYPE OF REPORT & PERIOD COVERED: PHD 論 THESIS
6. PERFORMING ORG. REPORT NUMBER	
7. AUTHOR(s): ROBERT V. PIERI	8. CONTRACT OR GRANT NUMBER(s)
9. PERFORMING ORGANIZATION NAME AND ADDRESS: AFIT STUDENT AT: CARNEGIE-MELLON UNIVERSITY	10. PROGRAM ELEMENT, PROJECT, TASK AREA & WORK UNIT NUMBERS
11. CONTROLLING OFFICE NAME AND ADDRESS	12. REPORT DATE: 1988
	13. NUMBER OF PAGES: 94
14. MONITORING AGENCY NAME & ADDRESS (if different from Controlling Office): AFIT/NR, Wright-Patterson AFB OH 45433-6583	15. SECURITY CLASS. (of this report): UNCLASSIFIED
	15a. DECLASSIFICATION DOWNGRADING SCHEDULE

16. DISTRIBUTION STATEMENT (of this Report)

DISTRIBUTED UNLIMITED: APPROVED FOR PUBLIC RELEASE

DTIC ELECTE AUG 0 3 1988 S D

17. DISTRIBUTION STATEMENT (of the abstract entered in Block 20, if different from Report)

SAME AS REPORT

18. SUPPLEMENTARY NOTES

Approved for Public Release: IAW AFR 190-1
LYNN E. WOLAVER 21 July 88
Dean for Research and Professional Development
Air Force Institute of Technology
Wright-Patterson AFB OH 45433-6583

19. KEY WORDS (Continue on reverse side if necessary and identify by block number)

20. ABSTRACT (Continue on reverse side if necessary and identify by block number)

ATTACHED

DD FORM 1 JAN 73 1473 EDITION OF 1 NOV 65 IS OBSOLETE

UNCLASSIFIED

SECURITY CLASSIFICATION OF THIS PAGE (When Data Entered)

SIZE EFFECTS IN LINEAR ELASTIC FRACTURE MECHANICS

ROBERT V. PIERI

ABSTRACT

In this study, we attempt an appraisal of the predictive ability of Linear Elastic Fracture Mechanics (LEFM) with respect to size scalings. We begin by describing the basic tenants of LEFM and what they would predict for three specific scaling problems. These problems are in-plane and out-of-plane scaling of a brittle material, each in a monotonic loading situation, and overall scaling in a constant stress, cyclic loading situation. Then the current literature is reviewed for experimental data applicable to these problems. These findings are presented in tabular and graph form and discussed. Next, three series of experiments are described, which are undertaken to augment the literature. Two of the series fracture common steel specimens in liquid nitrogen baths to obtain brittle response. The remaining experiments use aluminum alloy specimens to study cyclic loading with constant stress cycles. The study concludes by summarizing the ability of LEFM to deal with the problems, the resulting implications, and possible actions to overcome them.

CARNEGIE-MELLON UNIVERSITY

SIZE EFFECTS IN LINEAR ELASTIC FRACTURE MECHANICS

A DISSERTATION
SUBMITTED TO THE GRADUATE SCHOOL
IN PARTIAL FULFILLMENT OF THE REQUIREMENTS

for the degree

DOCTOR OF PHILOSOPHY

in

MECHANICAL ENGINEERING

by

ROBERT V. PIERI

Pittsburgh, Pennsylvania
October 1987

SIZE EFFECTS IN LINEAR ELASTIC FRACTURE MECHANICS

ROBERT V. PIERI

ABSTRACT

In this study, we attempt an appraisal of the predictive ability of Linear Elastic Fracture Mechanics (LEFM) with respect to size scalings. We begin by describing the basic tenants of LEFM and what they would predict for three specific scaling problems. These problems are in-plane and out-of-plane scaling of a brittle material, each in a monotonic loading situation, and overall scaling in a constant stress, cyclic loading situation. Then the current literature is reviewed for experimental data applicable to these problems. These findings are presented in tabular and graph form and discussed. Next, three series of experiments are described, which are undertaken to augment the literature. Two of the series fracture common steel specimens in liquid nitrogen baths to obtain brittle response. The remaining experiments use aluminum alloy specimens to study cyclic loading with constant stress cycles. The study concludes by summarizing the ability of LEFM to deal with the problems, the resulting implications, and possible actions to overcome them.

ACKNOWLEDGEMENTS

I have several people to whom I wish to express my gratitude. The first is my advisor, Professor G.B. Sinclair, whose support, guidance and example inspired me to complete this work. I also wish to thank other members of the Carnegie-Mellon community who have aided my efforts, notably the members of my thesis committee, this department's machine shop staff, my fellow graduate students, and the members of the Metallurgical Engineering and Materials Science department who allowed my many tests. In addition, I extend my thanks to Colonel Cary Fisher and others in the department of Engineering Mechanics at the United States Air Force Academy, who gave me the time and resources to bring this work to closure. The financial support of the Air Force and AFIT is appreciated.

And last, but never least, to my wife Pat, who typed the drafts and soothed the spirits,and my mother Francis, who shared the load, thank-you.

TABLE OF CONTENTS

Page

ABSTRACT ii

ACKNOWLEDGEMENTS iii

1. INTRODUCTION 1

2. LITERATURE REVIEW 11

3. MONOTONIC LOADING EXPERIMENTS 22

4. CYCLIC LOADING EXPERIMENTS 43

5. CONCLUDING REMARKS 50

REFERENCES 53

APPENDIX A. TABLES OF THICKNESS DATA 62

APPENDIX B. COOLING TIME CALCULATIONS 83

APPENDIX C. EXPERIMENTAL DETAILS 89

1. INTRODUCTION

This chapter discusses the basic issues of the thesis. We begin by describing fracture mechanics and discussing why it is important. We continue with a brief explanation of linear elastic fracture mechanics and go on to discuss scaling and why it is important. Then we outline the size predictions that are obtainable from LEFM for three particular situations. After this we define the objectives of the present work and finally we give a section-by-section listing of the topics to be covered herein.

One way to discuss fracture mechanics is to realize that objects are made from materials that are not perfect. These imperfections or defects can cause many things to happen. The thing that is of importance here is that these defects can cause a local stress increase in the object. The amount of this stress increase is related to the geometry of the defect itself and the object within which it is contained. As the geometry of the defect becomes more acuminated, the local stress begins to approach infinity, *i.e.* there is a stress singularity. This analytical result creates a conflict with experience since there is common knowledge of items containing sharp, crack-like features, which indeed do not break when exposed to the slightest of loadings. Fracture mechanics addresses itself to this inconsistency. A more formalized definition, based upon material defects, is given by Kanninen and Popelar [1], p. 89.

> "Fracture mechanics is an engineering discipline that quantifies the conditions under which a load-bearing solid body can fail due to the enlargement of a dominant crack contained in that body."

Some indication as to why one might be interested in fracture mechanics is highlighted in reports by Duga et al. [2] and [3]. These references cover a study conducted by Battel Laboratories for NBS in which the cost of fracture in the U.S. is placed at 119 billion dollars (1982 $) per year which is approximately 4 per cent of our Gross National Product. This study also indicated that 80 per cent of that total is associated with efforts to prevent fracture, as opposed to simply replacing broken parts. The study states that if the newest fracture mechanics

technologies were applied to manufacturing techniques, then $35 billion of this total could be saved. Based on these numbers one can see that it would be economically prudent to be able to better understand fracture mechanics.

The most fundamental and oldest portion of fracture mechanics is that dealing with the response of a linear elastic, or brittle material, linear elastic fracture mechanics, LEFM. An enjoyable history of its development is given by Kanninen and Popelar [1]. LEFM is based upon the use of a parameter called a stress intensity factor, K, to predict fracture. The stress intensity factor, K, is defined to be a coefficient of the singular stress field. In general, the form of K, as shown by Broek [5] and others, is,

$$K = \sigma \sqrt{a\pi}\, Y\left(\frac{a}{W}\right), \qquad (1.1)$$

where σ is the nominal applied stress, or the far-field stress. The a is the size of the defect or half crack length. And $Y(\frac{a}{W})$ is a geometry function describing the shape of the part; it is based upon the ratio of defect size to the nominal specimen size or width, W. LEFM says that when this K value reaches a particular level, the material fractures. The result is that by computing the stress-intensity factor for a particular load, and object geometry, one can determine if a fracture could occur by comparing the K value to a minimum critical stress-intensity factor, K_{1c} for the material†. However, this requires an elastic material response, that is to say, there should be no plastic deformation in the material. In applications, however, LEFM is used if any region of plastic deformation is confined to some relatively small distance around the defect.

---

† The parameter K is defined for three modes of loading, as shown in Rolfe and Barsom [4]. K_{1c} is the minimum critical stress intensity to occur for mode one or the crack opening mode, in plane-strain.

As with most technologies, the usefulness of LEFM is greatly enhanced if it can be applied to a broad range of specimen sizes. The ability to change with size or scale and still maintain its applicability is a basic requirement in predictive engineering methods. This ability to withstand scaling allows a technology to be applied from situation to situation, and in particular it allows a technology to be applied from a small scale laboratory testing situation to an application within the real world. By way of illustration, consider the difficulties of doing a full-scale test on the wing of a Boeing 747.

This study will look at the question of scaling in LEFM, and in particular, the effects of scaling on two distinct types of loading situations. The first is monotonic loading, basically used to determine the maximum load that a particular geometry can withstand or the critical stress intensity factor for a material. And the second situation is that where the loading oscillates, or cycles. The cyclic type of loading, usually called fatigue, is important because it determines the useful lifetime of a particular part at a load, or conversely, the load able to be endured for a required time span.

The monotonic scaling question can be broken out into changes in two separate dimensions, one being how wide the part is or its planar size, which we will call in-plane scaling. This is represented by Figure 1.1. As can be seen in this figure both width and defect size scale. In a similar fashion in Figure 1.2 is shown scaling in the remaining dimension, or out-of-plane scaling. Note that in this figure, the frontal view of the specimen does not change, but its thickness does. On the other hand for scaling under cyclic loading, we consider scaling without in-plane or out-of-plane separations. Therefore, the scaling here might be thought of as an overall-scaled or total-scaled situation. This geometry is represented in Figure 1.3.

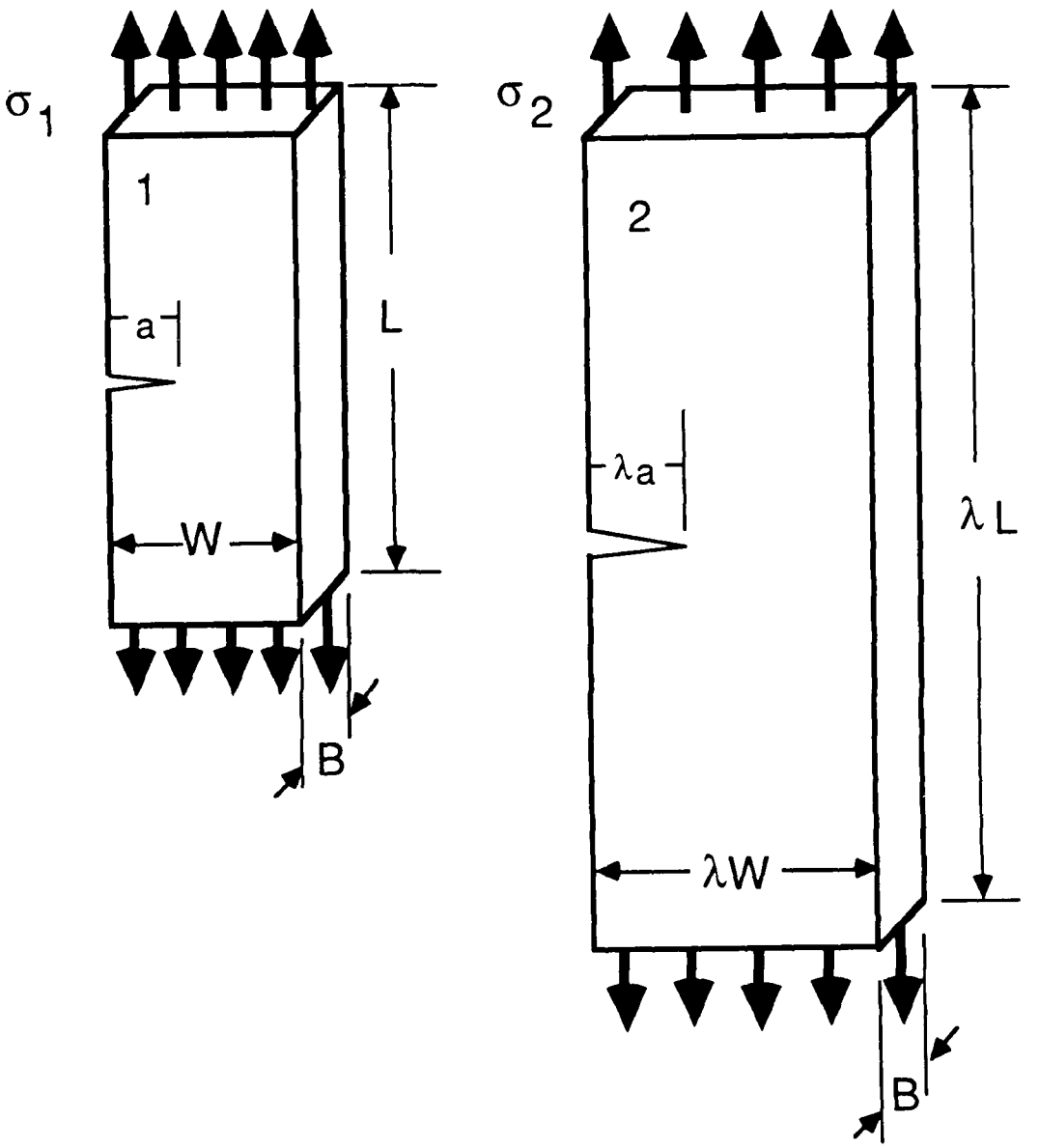

Figure 1.1 In-plane scaled specimens for monotonic loading.

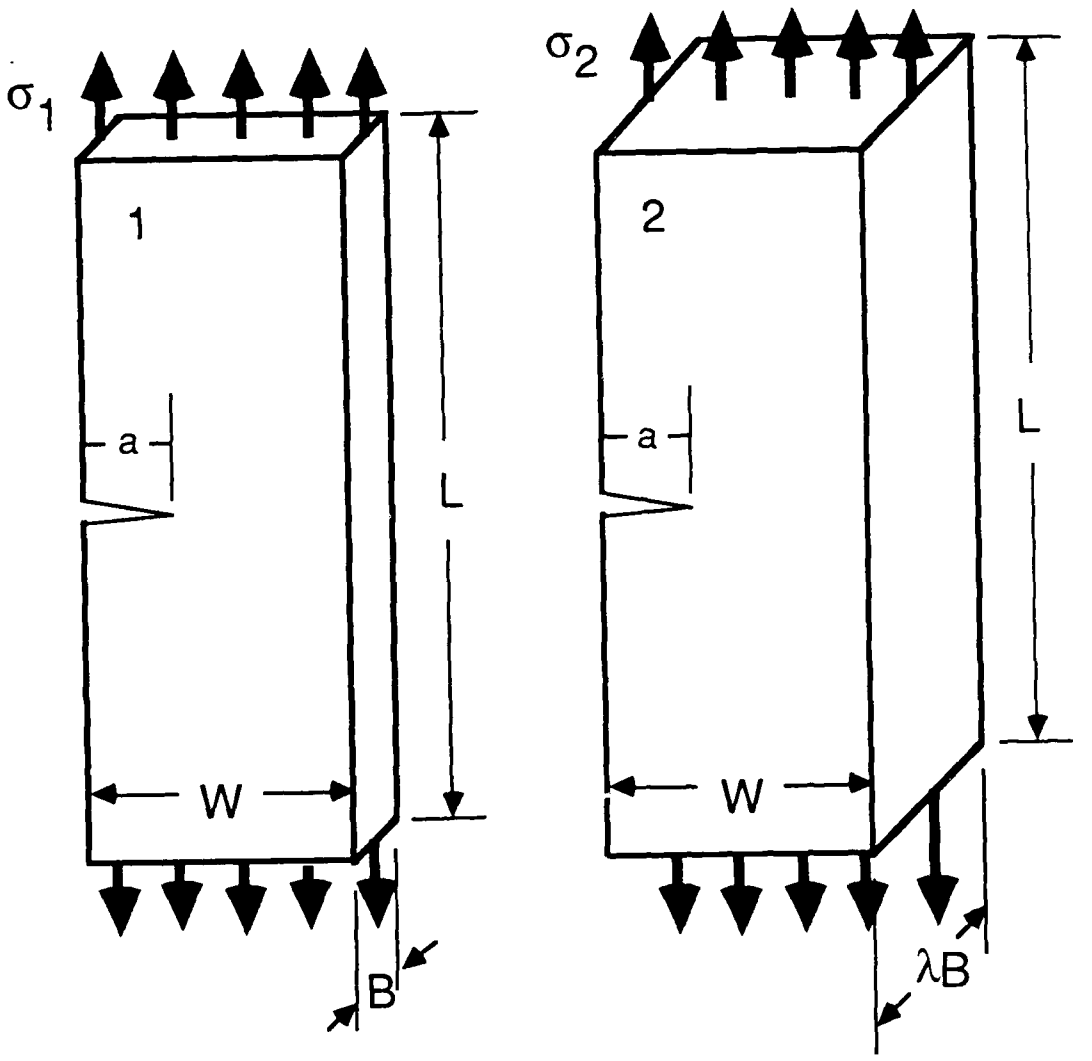

Figure 1.2 Out-of-plane scaled specimens for monotonic loading.

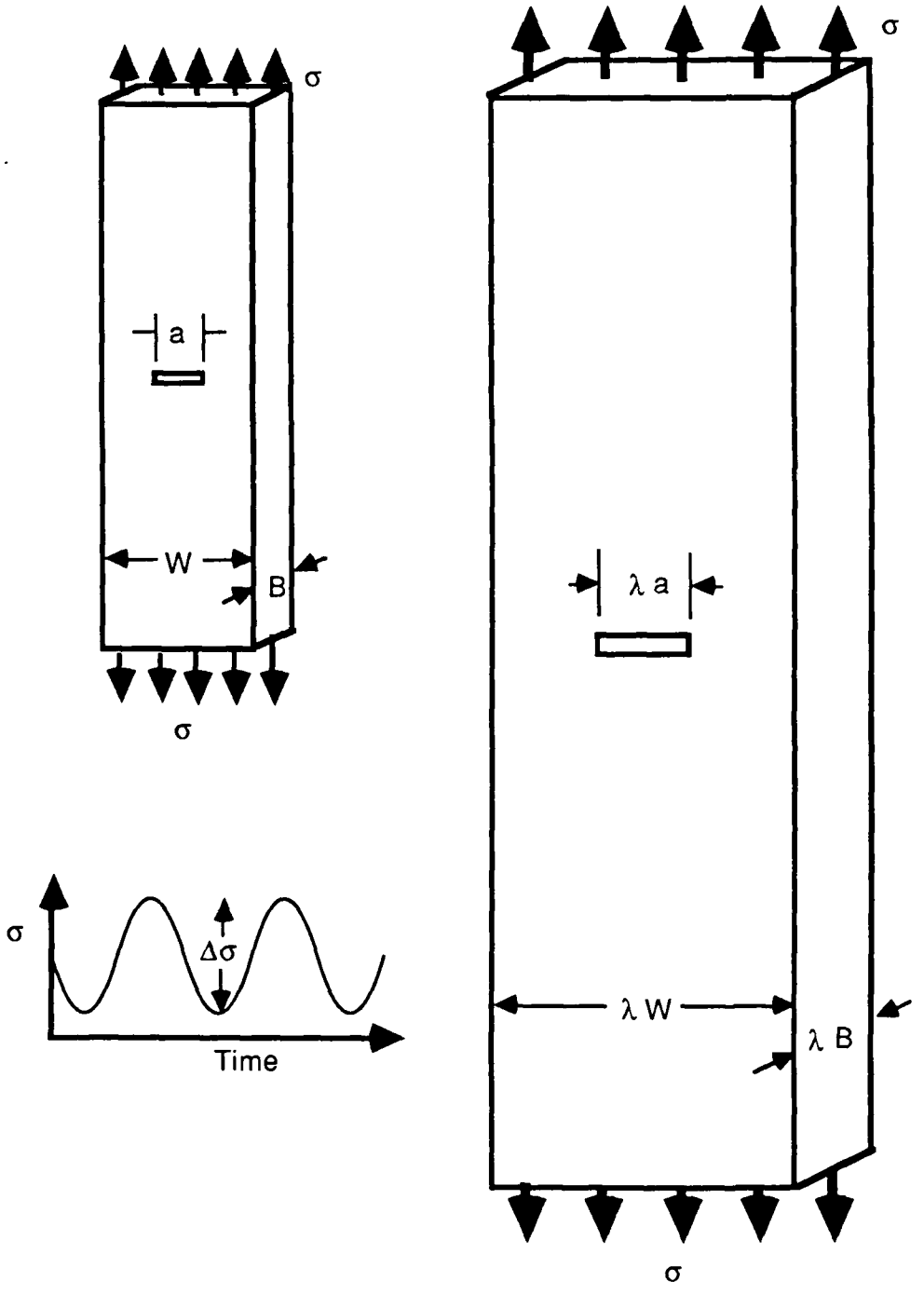

Figure 1.3 Scaled specimens for cyclic loading.

Now we go on to discuss what LEFM predicts as the scaling effects in each of these three situations. Addressing first the in-plane scaling effect for the monotonic loading situation, if one writes (1.1) for each of the two sizes of Figure 1.1, one gets,

$$K_1^* = \sigma_1^* \sqrt{a\pi}\, Y(\frac{a}{W}) \quad \text{and} \quad K_2^* = \sigma_2^* \sqrt{\lambda a\pi}\, Y(\frac{\lambda a}{\lambda W}). \qquad (1.2)$$

Here, the superscript * indicates a critical or fracture value. LEFM assumes that in both sizes failure occurs at the same critical K value if the specimens are made of the same material. This allows one to equate K_1^* and K_2^* in (1.2) and obtain the expression for the strength ratio as,

$$\frac{\sigma_1^*}{\sigma_2^*} = \sqrt{\lambda}. \qquad (1.3)$$

What (1.3) says is that as the cracked specimen gets bigger (λ>1), the stress at which it fails, or its strength, gets smaller relative to its strength for its initial size.

We now turn our attention to the LEFM prediction for out-of-plane scaling in the monotonic situation, i.e. that demonstrated by Figure 1.2. Doing a similar operation as above for out-of-plane scaling, one sees that there is no explicit statement of B in (1.1), therefore, there is no difference between the critical strength of the thick or the thin situation. This is the accepted situation for perfectly brittle materials, or materials with limited ductility. However, this absence of thickness effect changes when the material exhibits a degree of ductility. First, consider a thin specimen, or one that is in a state of plane stress, that is where there exists significant stresses in two principal directions while stresses in the third direction are negligible. As the loading of this specimen is increased, the differences between these principal stresses also increases, thereby increasing the shearing stress. Large shearing stresses imply yielding, and this yielding blunts the crack tip, which lowers the stress intensification. A lower stress intensification requires more loading to cause fracture, therefore the fracture strength goes up. In contrast, consider the situation arising when a thick specimen is loaded. Here, there exists a state of plane strain, *i.e.* the stresses of the three principal directions are not zero. As the applied load is increased, the

differences among these stresses do not rise as quickly, and therefore the shearing stress is lower, as is the tendency for yielding. Since yielding is not available to reduce the stress intensification, the thick specimen fractures at a loading less than for the thin specimen. In light of this explanation, the critical value of applied load is expected to increase with reduced thickness, hence the critical value of the stress intensity is expected to increase with reduced thickness.

Finally, we turn our attention to the cyclic loading situation. The equation of importance in that situation is known as the Paris Law,

$$\frac{da}{dN} = C\,(\Delta K)^m \quad \text{for} \quad \Delta K_{min} < \Delta K < \Delta K_{max}\,. \tag{1.4}$$

This empirical equation, based on a data reduction scheme, shows that the crack growth per cycle, da/dN, is a function of the change in the stress intensity as the loading cycles from maximum to minimum, ΔK, and two material parameters, C and m. What this expression and others like it attempt to do is predict the growth rate of the defect from an initial size to the point at which the crack length, a, is critical; *i.e.* a gets large enough so that K of (1.1) exceeds the critical value. Equation (1.4) has a useful range based upon the change in stress intensity. That is to say, below some "threshold" ΔK_{min}, there is typically no crack growth, at least (1.4) does not apply for whatever growth there is, and above ΔK_{max} there is catastrophic failure. The usual means of employing (1.4) is to convert it to an expression for lifetime, or number of cycles, N, from an initial crack size, a_i, to size at fracture, a_f. Rearranging (1.4), substituting an expression for ΔK, and preforming the necessary integration gives,

$$N = \frac{1}{C[\Delta\sigma\sqrt{\pi}]^m} \int_{a_i}^{a_f} \frac{1}{[Y(\frac{a}{W})\sqrt{a}]^m}\,da\,, \tag{1.5}$$

where $\Delta\sigma$ is the difference of extremes of the applied stress during the cycle.

Essential for (1.5) to be useful in practice is the assumption in LEFM that C and m are independent of size or scale. Further, for successful predictions using (1.5), there is really an implicit assumption that the range of applicability of (1.4), ΔK_{min} to ΔK_{max}, is also independent of scale. Under these conditions it is interesting to examine what (1.5) has to say about the cyclic lives of small and large specimens, N_S and N_l, respectively. Puttick and Atkins [6] discuss this and they predict,

$$\frac{N^*_S}{N^*_l} = \lambda^{(m/2-1)} \qquad (1.6)$$

Equation (1.6) assumes a_i/W and a_f/W are the same in both sizes, as is $\Delta\sigma$. Provided m>2, the life of the small specimen is predicted to be greater than that of the big.

We are now in a position to better define the objectives of this work. The goal here is to attempt to do a critical appraisal of how well these accepted predictions from LEFM actually work. We feel that one of three options is likely to occur. The first is that LEFM does indeed work and, therefore, is a viable technology and needs no improvement. The second possibility is that the predictions are marginal, that is to say, that they produce the right general trends but are off less than an order of magnitude. This would imply that the technology is not without redeeming features but needs some reworking to improve its capabilities. The last possibility is that LEFM, as a predictive technology simply doesn't work. This would imply that it is not even correct in trends or magnitudes of numbers. To handle these last two outcomes is beyond the scope of the present work. To fully reconcile the complete body of data obtained over the last thirty to forty years under these circumstances would be a truly Herculean task, though some directions along which one might proceed in this event can be suggested.

The remainder of the thesis is organized as follows. The next chapter is a literature review for pertinent data. Following this is a description of a series of monotonic loading experiments after which we describe a series of cyclic loading experiments. The fifth section contains some

concluding remarks based upon the two experimental series. (Thickness data tables, a heat conduction analysis, and details of the experimental results are appended.)

2. LITERATURE REVIEW

In this chapter we present the results of a review of the literature pertinent to the questions of Chapter 1. We begin by discussing the literature that addresses in-plane scaling, and then go on to articles on thickness scaling. Finally, we conclude by looking at some papers that address the question of scaling in cyclic loading situations.

With respect to in-plane scaling, a recently completed local work, Sinclair and Chambers [7], comments upon how well the physical evidence compares to predictions based upon LEFM. After an extensive review of the open literature, the authors present six plots of normalized strength versus scaling factor which summarize their results for plane-strain or plane-stress and material response of brittle, brittle-ductile, or ductile . A typical curve is reproduced in Figure 2.1. This particular figure shows the plane-strain brittle response for a number of reported articles. The LEFM prediction of equation (1.3) is shown by the solid line, and the points represent reported results, large points indicating many experiments. As can be seen in this figure, the agreement between the prediction and the experimental results is not good. To quantify this statement, somewhat, LEFM is found to give predictions that are not within ± 10% of actual results over 80% of the time when the scale factor, λ, is greater than 3, and 100% of the time when $\lambda > 7$. The article concludes by stating that, although the results are trendwise correct, they tend to be too simplistic and that the net result is a need to test at various specimen sizes.

Now, we turn our attention to out-of-plane scaling. A search of the open literature was undertaken for results of experiments scaling thicknesses of otherwise identical specimens. To be compatible with the above article [7], many of the same guidelines are used when reporting the results. Comparison is made only within a single source and only to the extent that identical geometries (center-cracked tension,edge-notch bending, etc.),materials and environment are used. In-plane dimensions are required to remain constant for various

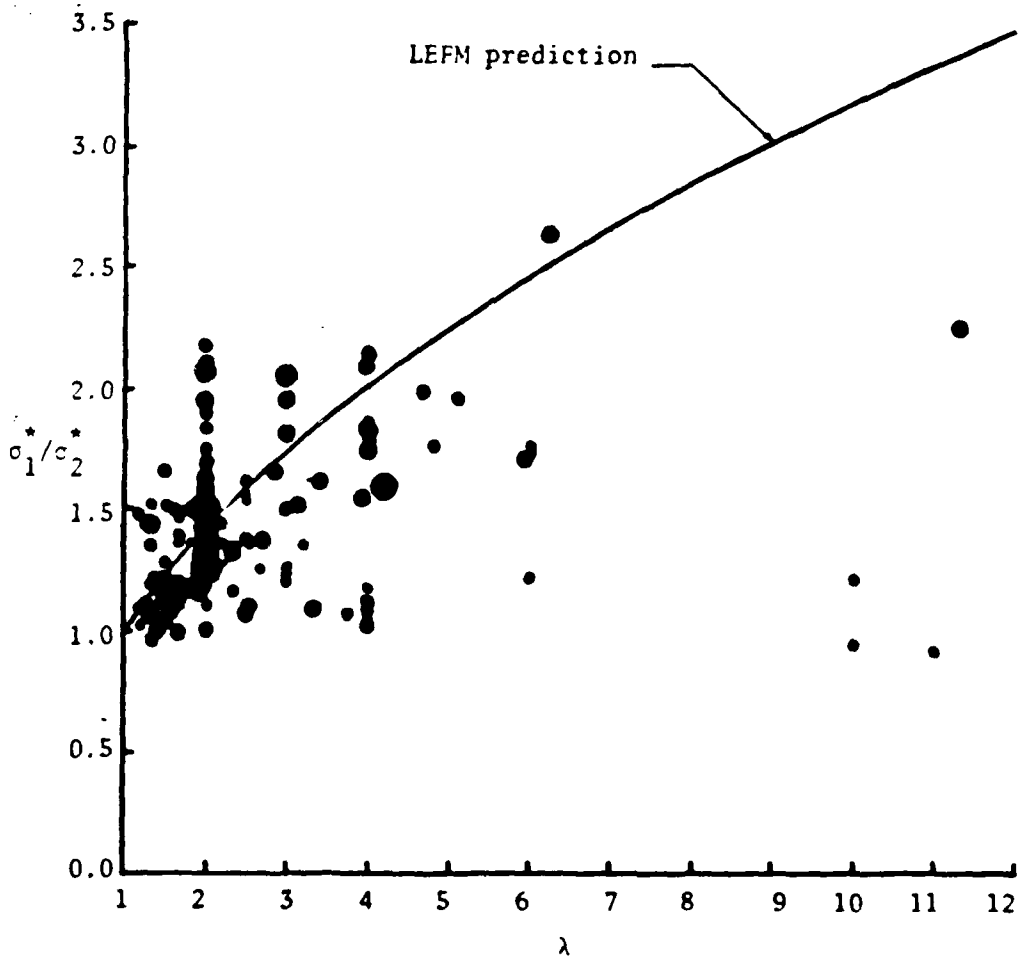

Figure 2.1 Normalized strength versus scaling factor for in-plane scaled experiments, plane strain, brittle response, from Sinclair and Chambers [7].

thicknesses used, although a small variation of crack length, a, is permitted; *i.e.*, $\Delta(a/W) < \pm 10\%$. Crack or notch acuity must be sharp as determined by the ratio of defect radius of curvature, ρ, to a; *i.e.*, $\rho/a \leq 0.1$: fatigue precracking is preferred. The material response is categorized into three regimes, based upon the relative plastic zone size, r_y/a; *i.e.* :

$$\begin{aligned} r_y/a &< 0.02 && \text{brittle;} \\ 0.02 \leq r_y/a &\leq 0.05 && \text{brittle-ductile, and;} \\ 0.05 &< r_y/a && \text{ductile.} \end{aligned} \qquad (2.1)$$

Relative plastic zone size is computed by using:

$$r_y/a = \frac{1}{2\pi a}\left(\frac{K_I}{\sigma_y}\right)^2 \quad \text{for plane stress, or}$$

$$r_y/a = \frac{1}{6\pi a}\left(\frac{K_I}{\sigma_y}\right)^2 \quad \text{for plane strain, or,} \qquad (2.2)$$

$$r_y/a = \frac{1}{4\pi a}\left(\frac{K_I}{\sigma_y}\right)^2 \quad \text{between the two.}$$

Here, σ_y is the yield strength of the material at similar conditions. The classification according to material response is done since a brittle response affords the best comparison with LEFM, and the brittle-ductile response is the natural place into which extension of the LEFM prediction is logical. Strength is taken as the nominal applied stress at the onset of Mode I crack growth. This can be inferred from energy release rate (G), stress intensity (K), or nominal net stress, although the preferred information is critical load and specimen geometry. If the only information given is at maximum loading, it was used, otherwise the values at 5% offset or at pop-in were preferred. This is done to get information at the onset of crack growth, when plastic deformation should be minimal.

After review of some articles, it became apparent that simply reporting strength versus thickness would not work. By way of illustration consider two experiments: in one, the in-plane

dimension is one inch and the thickness varies from 1/8 inch to 3/4 inch. In the other, the thickness varies in the same range, but now the major in-plane dimension is 12 inches. The point here is that the same thickness in one experiment will clearly be in a plane-strain regime, while, in another experiment, that thickness is in the plane-stress regime. To overcome this problem, we decided to characterize results based upon a dimension that would essentially define the plane-stress to plane-strain transition for all test specimens. To accomplish this, we somewhat arbitrarily use the ratio of thickness to crack length, specifically 2B/a as the transition parameter. This is comparable to the ASTM standard E399 [8] which uses the ratio of thickness to width to define plane-strain response. If the ratio 2B/a equals one for a configuration, then the specimen is taken to be at the transition from the plane-stress and plane-strain loading regions. If the ratio is two or better, then the response is plane-strain, while if the ratio is less than 0.2, the response is plane-stress. The reported strength is normalized by the strength for a specimen with a 2B/a ratio equal to one. If such a specimen was not actually reported, then the data is interpolated if possible, extrapolated where not, to the proper ratio. The basis for the interpolation/ extrapolation is a straight line on a log-log plot. Clearly, this is not the only way to handle this scaling situation, but, hopefully, it represents one rational way of doing it.

In the course of this phase of the work, in excess of 120 articles were reviewed for data. Of these, only 58 [9 to 67] contained enough data to allow comparison of relative strength to relative thickness . The remaining 62 articles [68 to 130] were such that, although they address the topic of out-of-plane scaling, they did not contain enough information to either calculate relative strength or size, or to compute the response of the material. Such articles are, though, included for completeness. Although this data search is probably not all-inclusive, it should give a feeling for the trend of the reported experimental results. The detailed information that could be obtained from these articles is contained in tables in Appendix A. This same information, classified as to material response, is plotted in Figures 2.2, 2.3, and 2.4.

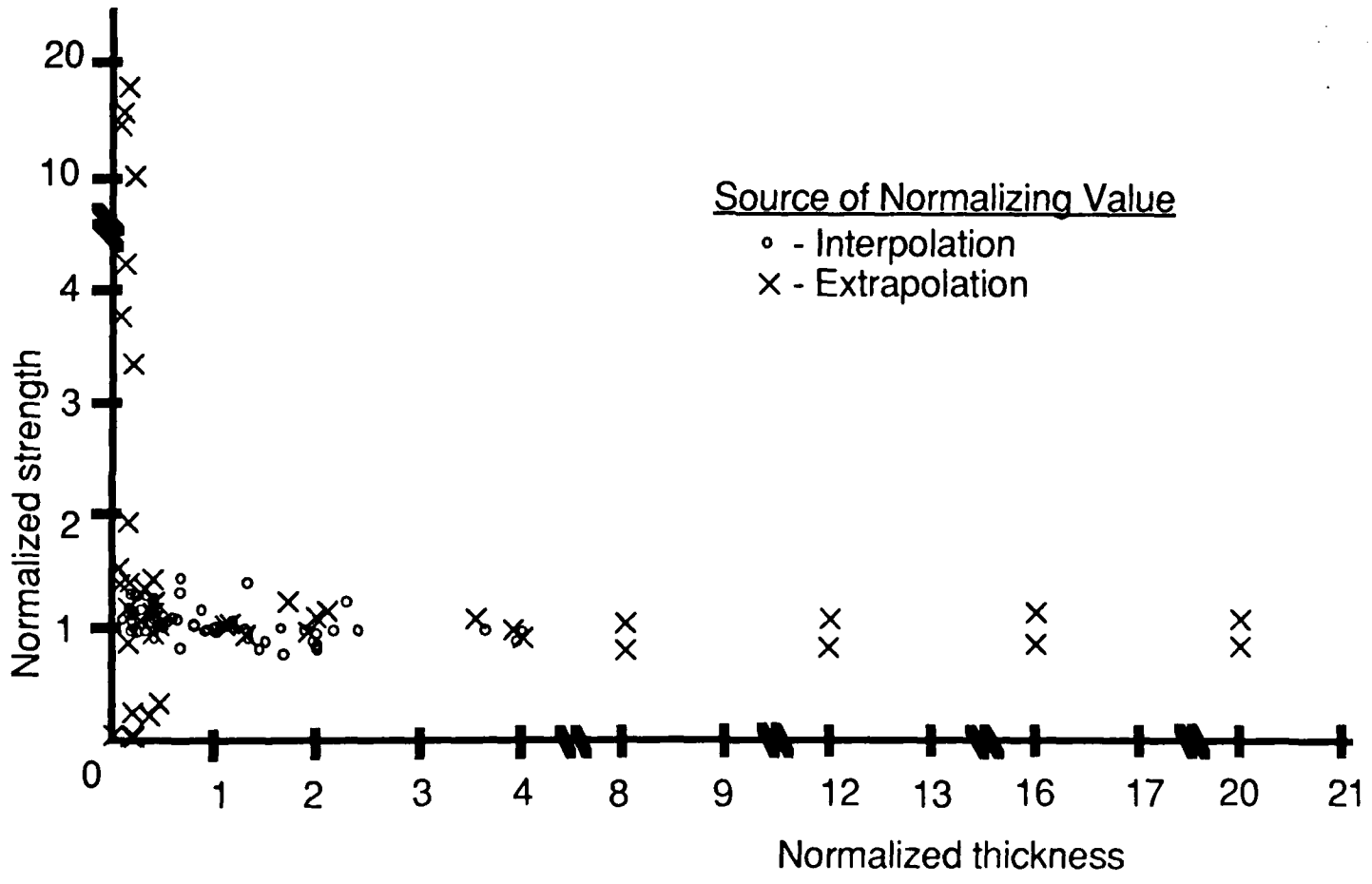

Figure 2.2 Plot of normalized strength vs. normalized thickness, Brittle response.

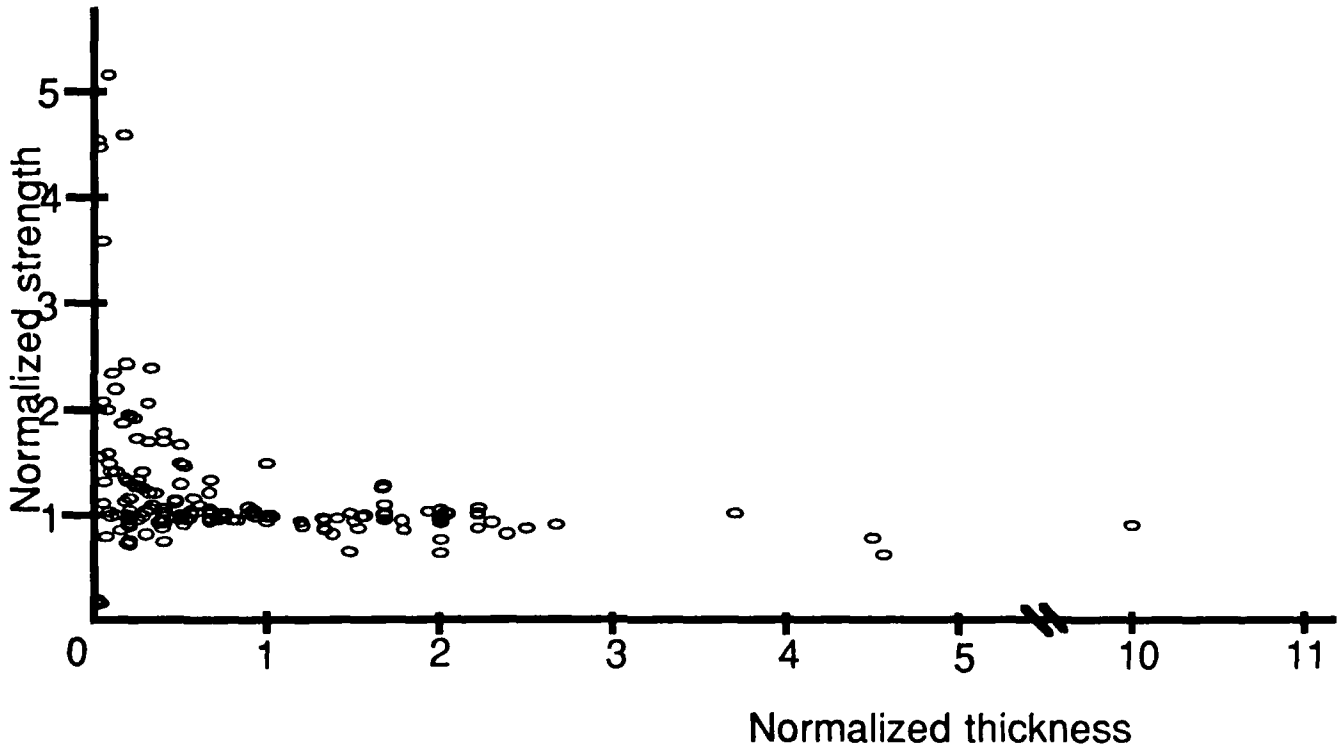

Figure 2.3 Plot of normalized strength vs normalized thickness, Brittle-ductile response.

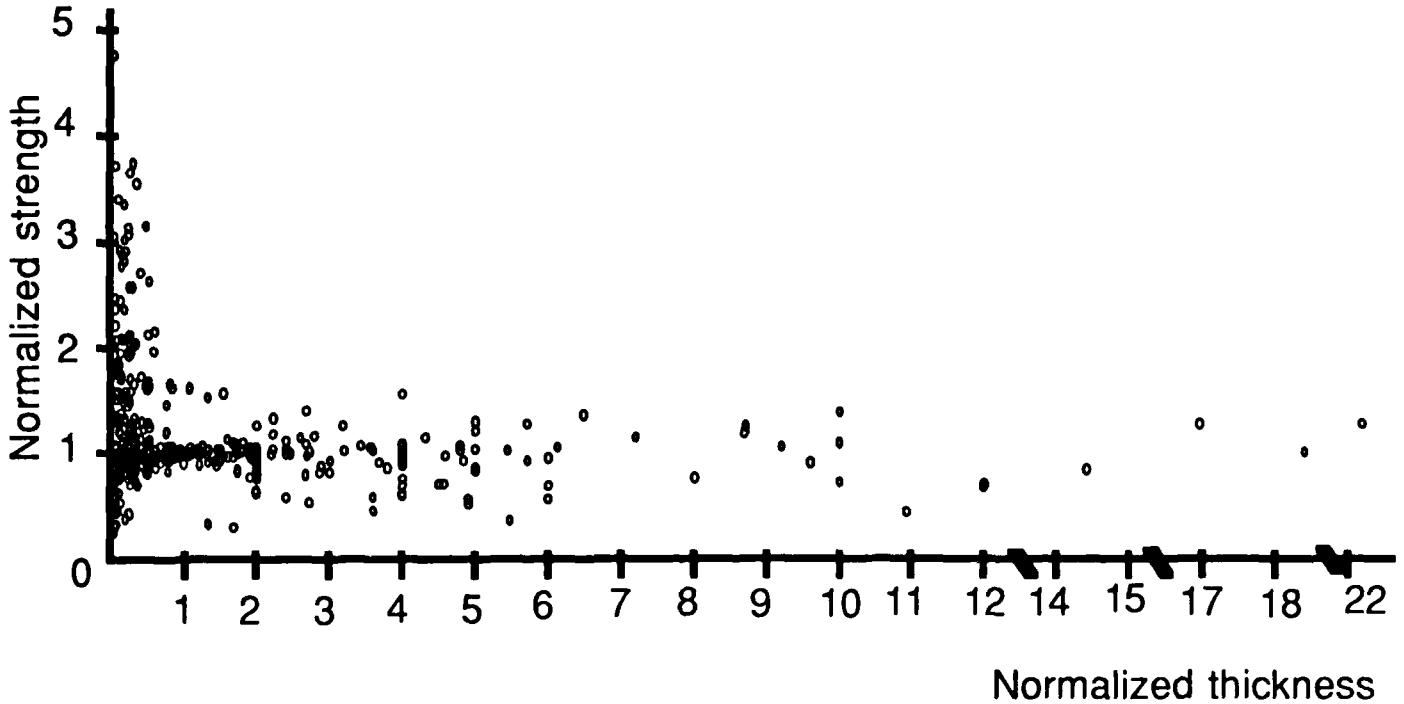

Figure 2.4 Plot of normalized strength vs normalized thickness, Ductile response.

Figure 2.2 presents the dependence of strength upon thickness when $r_y/a < 0.02$, *i.e.* brittle response, which should most closely fit the standard LEFM prediction. If this response determination where checked again using $r_y/B < 0.02$, it is possible that in some cases the thinnest specimens could no longer be classified as brittle. However, in order to include more data, we restrict ourselves to the r_y/a criteria. As can be seen, most of the data groups about a scaling factor of one, indicating that most of the testing is done in the plane-stress transition region. The LEFM prediction for this response is a horizontal line at a relative strength of one. As can be seen, the results oscillate above and below this prediction. Relatively few experiments are actually represented on this curve, and the range in any single experimental study is rather small. Presented for completeness are similar reported data for material responses in the brittle-ductile and ductile regimes, plotted in Figures 2.3 and 2.4, respectively. Note in both figures the larger number of data points and the larger range of reported results.

Based upon the above figures, one sees that the reported data for the brittle behavior of out-of-plane scaled experiments is not conclusive; that is, there is no clear trend in the existing data, as shown in Figure 2.2. Also, there is not a large number of experiments with brittle materials, and no single experiment showed a large scale factor. Thus, there appears to be room for another series of experiments in this area.

To conclude the data search, we now turn our attention to reported experiments on size effects for cyclicly loaded cracked specimens; that is, specimens which should be amenable to reduction by the Paris Law of Equation 1.4. This is not as fertile an area of publication as in the monotonic studies. Restricting our attention to specimen pairs of identical types made of a single material with both width and thickness scaled in concert, and which are tested at the same temperature, and loaded with as similar frequency and stress range as possible, six references with admissible data can be identified [131 to 136]. All of the data they contain are for steels and the units used for C are those consistent with expressing a in inches, and ΔK in ksi$\sqrt{\text{in}}$. These

data are summarized in Table 2.1, wherein λ is the scaling factor. Clearly, in Table 2.1, m and C can vary with size: what is not clear from Table 2.1 are the implications of these discrepancies from a cyclic life point-of-view. To obtain some idea of these consequences, we look to develop a ratio for the lives calculated using an expression similar to Equation 1.6. To do this and incorporate the data from Table 2.1, we use the expression for lifetime, N, given in (1.5). In adapting (1.5) to furnish the desired ratio, several simplifying assumptions are made. First, we set the function $Y(\frac{A}{W})$ equal to one to facilitate integration. Second, we take a_i as 1/32 in., a common initial flaw size taken in practice because of detection capabilities. Finally and somewhat arbitrarily, we let a_f be 1/4 in., a value which can occur in engineering applications and one which allows sufficient crack growth to have significant life. The end result is;

$$\frac{N_S}{N_l} = \left(\frac{C_l(m_l-2)}{C_S(m_S-2)}\right)\left(\frac{\Delta\sigma\sqrt{\pi}}{2}\right)^{m_l-m_s} \frac{8^{(m_S-2)/2}-1}{8^{(m_l-2)/2}-1} \qquad (2.3)$$

where the subscripts l and s refer to values associated with the larger or smaller specimens, respectively, i.e., m_S is the exponent reported for the smaller specimen. With this equation, we get a feel for the impact of changes with size.

We now evaluate (2.3) using the parameters given in Table 2.1 and representative values from the particular sources. We see that the resulting ratio may be greater or less than unity. Cases where N_S/N_l is greater than one may be interpreted as implying a conservative estimate of life if m, and C found via testing the larger specimen were used to predict life in the smaller, but nonconservative if the smaller specimen provided parameters to predict life in the larger. Hence one immediate consequence is that neither testing small and applying big nor vice versa ensures a conservative result. To emphasize the potential for nonconservative estimates, we give results from (2.3) as numbers equal to or greater than one, inverting the ratio when needed, and then assume that the denominator represents the size used to

Table 2.1 Paris law parameters for scaled specimens.

Be#	λ	m	C (x10^{10})
131	1	2.25	32.4
	2	2.24	57.9
	1	2.16	58.9
	2	2.18	24.1
	1	2.16	77.5
	2	2.13	75.2
	1	2.48	12.1
	2	2.54	14.8
132	1	3.67	0.60
	2	3.98	0.10
	4	3.57	0.40
	1	3.28	1.60
	4	3.24	0.97
133	1	2.03	44.6
	2	2.21	23.1
	3	2.06	45.6
	4	2.23	23.7
134	1	2.7	46.1
	2	2.2	24.5
	1	3.1	1.76
	2	1.9	91.0
135	1	3.09	1.80
	2	3.48	0.40
	1	3.02	3.00
	4	2.81	4.70
136	1	5.44	0.00075
	4	4.33	0.0313
	1	3.27	0.18
	4	3.23	0.23

predict the lifetime of the size represented by the numerator. Thus we get numbers that are the multiplicative factor by which one would over predict actual life, *i.e.* N_S/N_l implies the over predicted life of a small specimen based upon calibrating a large. These factors then are as follows.

Parameters from N_I/N_S; 1.8, 1.3, 2.4, 45.0, 1.1, 36.0, 1.3

Parameters from N_S/N_I; 2.4, 1.1, 1.9, 1.7, 1.9, 2.6, 1.6, 2.2, 1.6

We can now grade these results by making the modest requirement that errors less than a factor of two are satisfactory results, then regard results greater than two, but less than four, as poor, and those larger than four as quite inadequate. Based on this, the above represents satisfactory predictions 62% of the time, poor predictions 25%, and inadequate 13%. Clearly there is room for improvement.

In this review of the physical evidence, several lacunas exist with respect to our objective of gauging how well the Paris data reduction scheme performs on specimens that are merely scaled. None of the cited references reported using exactly the same cyclic stress loading in each of their different sizes. None of them either involved sufficient repetition of tests or presented results in such a way as to enable a good assessment of the degree of scatter present. And none of them really allowed the effects of changing sizes on the end points of the data fit, ΔK_{min} or ΔK_{max}, to be discerned. Accordingly, we consider a set of experiments designed to filling these gaps, as well as those of the monotonic studies, mentioned earlier.

3. MONOTONIC LOADING EXPERIMENTS

In this chapter we describe a series of experiments with the goal of showing how out-of-plane scaling effects the fracture behavior of a material. We begin by describing a preliminary experimental study, the over-all design objectives for these experiments, and how they are implemented. The discussion then goes on to the results obtained from these preliminary experiments, and how these results lead to an extended series of experiments, designed not only to explore out-of-plane scaling, but also to see if a correlation might exist with in-plane scaling. The chapter concludes with a presentation of data obtained from this expanded series of experiments.

3.1 Preliminary experimental study

The most important design objective is to be sure that the experiments do in fact focus on the effects of out-of-plane scaling upon LEFM. Clearly this is done by building a series of experiments in which the only dimension change is that of the thickness, B.

The next most important objective is that the material used exhibit as brittle a response as possible, since this response affords the best comparison with LEFM by virtue of complying with the underlying assumptions best. However, seeking a brittle material does present difficulties in that it is typically costly to procure in high quality form, and hard to machine into finished specimens. A way around these problems is to use a material that could, in one instance, be ductile for specimen preparation, but in another instance be brittle for testing. One means to have these two features would be to take advantage of a temperature transition in a material. It is known that medium content carbon steels can behave in such a manner. At normal room temperature these steels are ductile and easily machined, while if immersed in liquid nitrogen (77° K) they now exhibit brittle response. It is recognized that this behavior will have to be confirmed via a tensile test at fracture, and a description of this is below. An additional advantage to using this steel is

that it is a well known structural material having a rather wide range of applications as opposed to a material like Alumina. The actual steel chosen is AISI 1045.

Another important design consideration is obtaining reliable results. That is to say, being able to discern real material response from experimental noise. Two approaches are used to address this question. One is to use a large scale factor, changing B by a factor of ten or more. In this way it is hoped to accentuate any real physical thickness effects present. And the other approach is to test enough specimens so as to be able to estimate in a statistical fashion the scatter of the results obtained.

From the onset we also want these experiments to follow as closely as possible the intent of ASTM standard E 399 [8]. We do this because this standard has achieved quite a degree of acceptance with the fracture mechanics community and because it generally represents a good method for obtaining reproducible results. It is not without some work that one is able to incorporate this objective since the standard has eleven criteria to be met. Most criteria do not change; for example: planar dimensions, recording and reporting requirements, and measuring methods. None the less, some criteria were harder to keep on a consistent basis, as the total critical crack length, a_c, and therefore the ratio of crack length to specimen width, a_c/W. The criteria that was impossible to meet was, of course, the minimum thickness requirement for plane strain testing.

It is decided that a disk shaped compact specimen should be used for the fracture tests, Figure 3.1. This circular specimen allows minimum trim loss of materials, and facilitates fabrication procedures. Once a particular diameter is settled upon, different thickness are obtained by simply slicing off a length of stock rod material roughly equal to the desired thickness. Having in mind testing load capabilities, we choose a diameter of 2 inches. Thereafter, machining is used to cut mounting holes, the initial crack, and bring the specimens to final thickness. Eight specimen thicknesses are produced, from 3 inches down to 3/64 inches, with between 2 to 4 specimens in

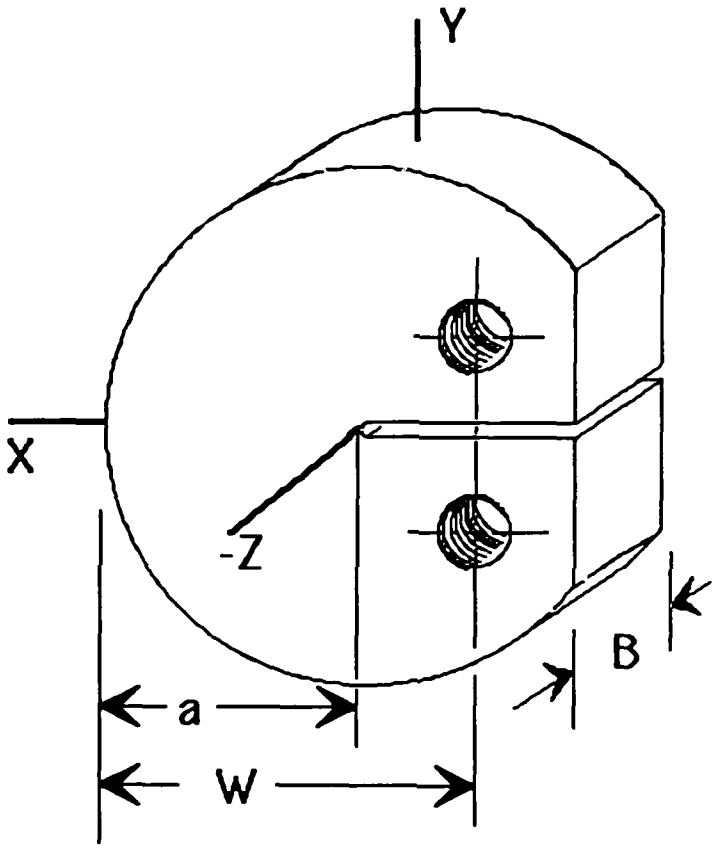

Figure 3.1 Compact disk geometry.

each thickness. The smallest specimens need considerable care to keep aligned so that no extraneous bending stresses are introduced. Hence a relatively large sample number, 8 specimens, are prepared to try to check that these stresses were not present. (A summary showing thicknesses and numbers tested is in Appendix C.)

To gauge the effects of machining, about half of the specimens are tested in the "as-received" state while the other half are heat treated to reduce residual stress introduced during fabrication. The heat-treating is such as to restore the material to a "dead anneal" condition (see Metals Handbook [137], pp 14-27). This is accomplished by inserting the specimens into an argon atmosphere furnace and raising their temperature to just above 1500°F, holding it until equilibrium is reached (one to two hours depending upon specimen thickness), and then decreasing the temperature at 50 degrees per hour until 1200 °F, when the oven is shut off.

After heat-treatment, all the specimens are fatigue precracked in order to grow a sharp radiused crack. The length of the fatigue precrack is such that the ratio of total crack length, a, to width, W, is within the desired range, here 0.53 to 0.55. This produces adequate crack growth with respect to the ASTM standard[8] The precrack length is measured using a traveling microscope. During this fatigue precracking, the maximum load is held within limits as defined in ASTM E399 [8].

The actual fracture test is now able to be conducted. The specimens are mounted in an MTS 55kip servo-hydraulic testing machine, Plate 3.1. A simple liquid nitrogen container designed to this end is then assembled around the specimen. Once this is secured, liquid nitrogen is poured into the container until it covers the specimen, and is kept there until the specimen reaches a uniform temperature as based upon analysis (see Appendix B for temperature calculations). This test setup uses between five and twenty liters of liquid

Plate 3.1 Specimen for monotonic loading.

nitrogen, depending upon thickness, to cool the specimens. The hold time is confirmed by noting the boil off of liquid around the specimen. The testing machine is then programed in load control to apply a steadily increasing load at a rate such that the specimen experiences an increase of the stress intensity factor equal to 130 ksi$\sqrt{in}$ /min until fracture, within limits set in ASTM E399 [8]. The system records output from the load cell as well as the displacement, or stroke, of the hydraulic ram. The load vs stroke curve is recorded.

After the broken specimen halves have warmed up, they are measured to determine the critical crack at fracture. Since the demarcation between fatigue crack and precipitous growth to failure is usually obvious, it was fairly easy to comply with ASTM E399 [8] requirements for measuring the final crack front at the center and 'quarter-thickness' points. The average of these values constitutes a_c and can now be combined with three other measurements, namely specimen width (W), thickness (B) and load at failure (P^*), to obtain net nominal stress at fracture, σ_n^*. The net nominal stress for this shape specimen is obtained by remembering that the stress in this remaining ligament results from both normal and bending loading therefore the following applies: $\sigma_n^* = (P^*/(B(W-a))\ (1+ 3(W+a)/(W-a))$. The value for σ_n^* is now normalized with that for the largest specimen and plotted against thickness value, also normalized with respect to the largest specimen. It is interesting to note that since the in-plane dimensions are constant, the variation of thickness constitutes a variation of volume in the specimens. Thus, this plot of normalized net nominal stress, σ_N^*, can be drawn as versus thickness or gross volume, V, where $V= \frac{\pi}{4} BW^2$.

As stated above, the brittle nature of the response has to be confirmed by obtaining the stress-strain curve for the 1045 steel at this testing temperature. Four specimens are constructed following ASTM standard E8 [138], see especially figure 7 there. The rectangular cross section of these specimens is 0.5" by 0.19", and the distance between mounting pins is 5". After manufacture, these tensile specimens are heat-treated in an identical procedure to the fracture specimens. The tensile tests are carried out in a fashion similar to the liquid nitrogen fracture

tests. Results recorded included the load displacement curve, yield stress, and reduction in area at fracture.

Turning to the results obtained, we first note the information from the fracture tests. The typical load vs stroke curve is uniformly linear, after an initial section to relieve play in the load train, Figure 3.2. This response is consistent with desired brittle behavior. Also consistent with brittle response is the absence of shear lips on any of the cooled specimens, all had essentially flat fracture surfaces. It is believed that this is indicative of brittle materials, as mentioned in Knott [139] and others. Measuring the fractured surfaces showed that none of the thickest specimens have a/W ratios within the desired range. In addition, all specimens are checked for compliance with the crack front curvature requirements of ASTM standard [8]. It is noted that crack front shape is different in the various thicknesses, therefore, the relationship of surface crack size to a_c varied.

The plot of normalized net nominal stress vs normalized gross volume is shown in Figure 3.3. In this figure is shown experimental results for specimens that are either heat-treated or not. Specimens who's a/W ratio is not within the desired range are identified in Figure 3.3. The curve of Figure 3.3 shows no major differences between the behavior of annealed or non-annealed specimens. Both start at a low critical stress, and as the volume decreases, the strength increases. (Details of results for all cases are in Appended C.) If these results were for perfectly or nearly perfectly brittle response, then they really do not conform with LEFM. This is because LEFM attributes thickness effects to changes in ductility and otherwise has that there are no effects.

Lastly, then, we consider the check on brittleness. The results of the tensile tests show that the yield strength at liquid nitrogen temperature was approximately 135 ksi. However, upon inspection, the tested specimens showed excessive amounts of reduction in

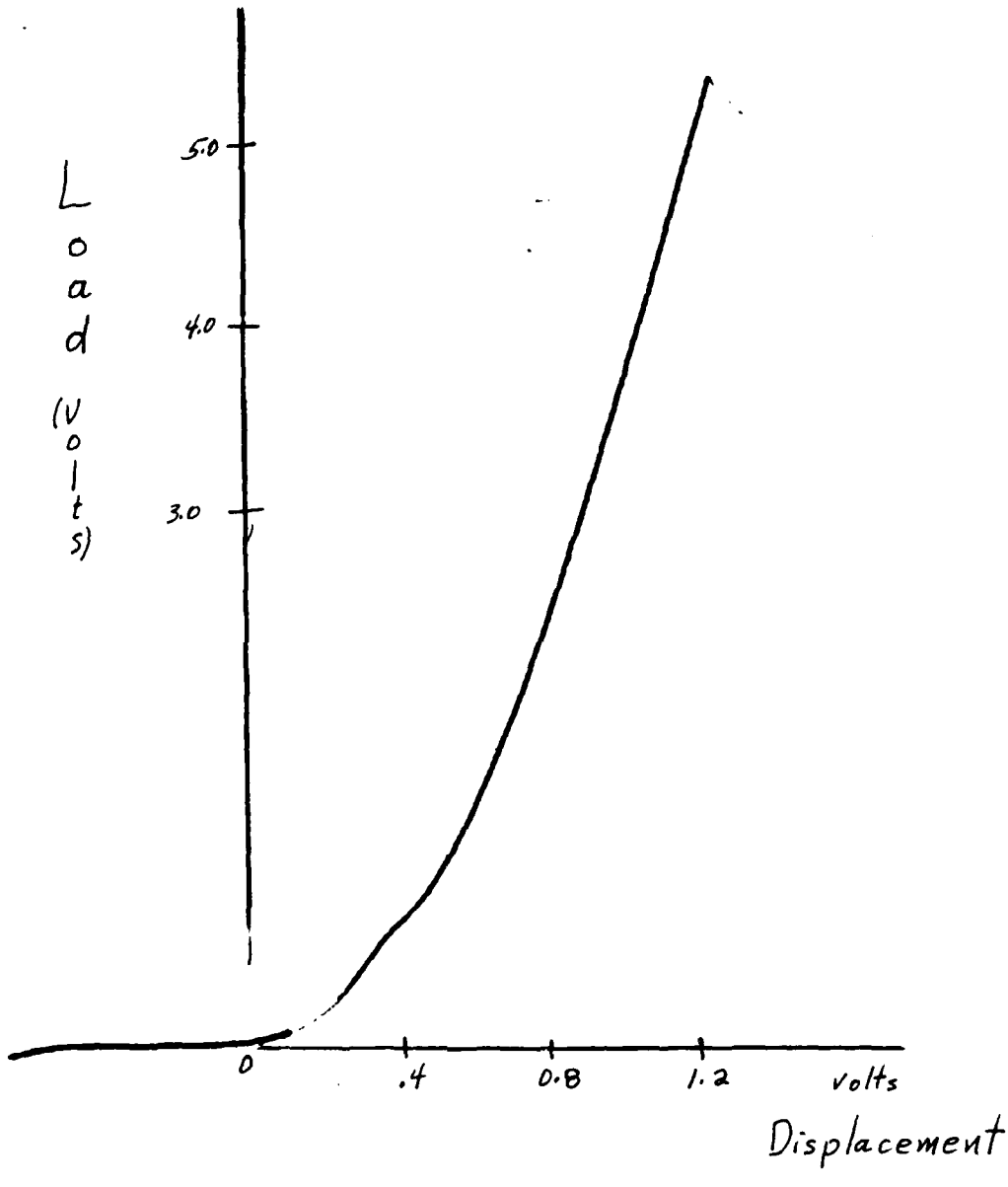

Figure 3.2 Typical load versus diplacement curve for monotonic test.

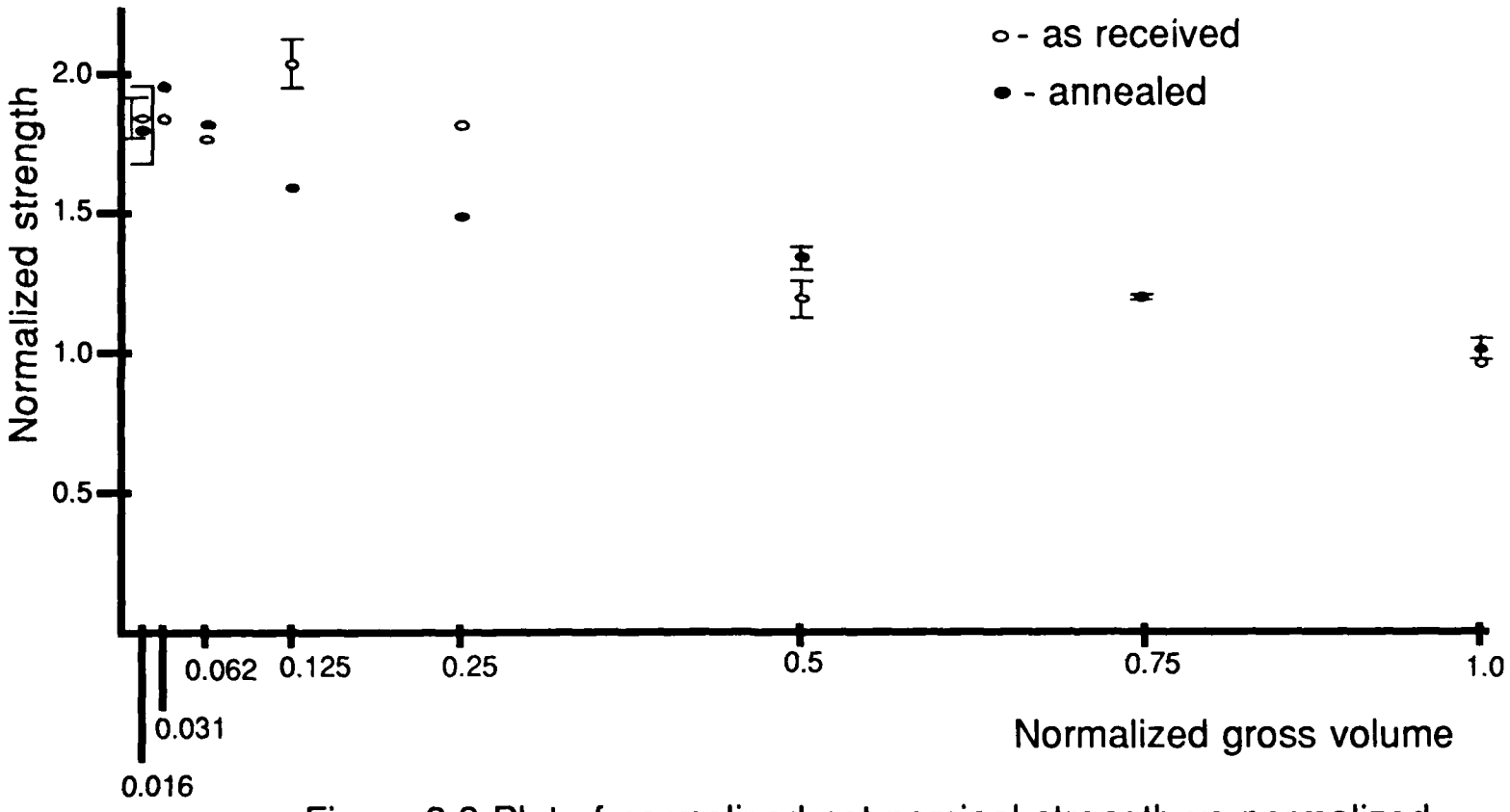

Figure 3.3 Plot of normalized net nominal strength vs normalized gross volume, preliminary study

area, approximately 39 %. This would imply that the specimens actually failed in a ductile fashion as opposed to brittle. These results led to some questioning of the material selection process. Microphotographs of these tensile specimens show a marked difference in the material from the surface towards the interior, Plate 3.2. Such a situation could come about as carbon in the steel is lost via diffusion during the heat-treatment. A loss of carbon turns a 1045 steel into a 1020 or 1010 type, having more ductile properties. As a result, these preliminary experiments failed to meet our objective of brittle response. They do, however, show an alternative which might be successful and we explore this next.

3.2 Extended experimental study

In light of the above findings, a second extended series of experiments are undertaken with changes made in the specimen preparation and pretest handling. This time the raw stock is annealed first and then the specimens fabricated from it. In this way the region containing the migration of carbon atoms referred to above can be machined off.

At the same time as enacting these preparation changes, it is desirable to extend the preliminary experiments from simple out-of-plane considerations so as to explore the possibility of a correlation between in-plane and out-of-plane scaling, and how this might relate to the nominal volume of the cracked specimen. This extension of the experiments can be carried out relatively easily by having the specimen dimensions change, not only in thickness direction, but also in the planar, or width (W) direction. The selection of specimen width and thicknesses are done in a fashion so as to admit some common volumes for different combinations of dimensions. In particular, for example, the thickness of the thinnest large-diameter specimen is chosen such that it has the same volume as the second thickest specimen of the next smaller diameter. In a particular planar size, the thicknesses usually change by a factor of two. In total, three diameters were chosen, 1 inch, 2 inches, and 4

Plate 3.2 Microphotograph (100×) of tensile specimen showing loss of carbon rich phase near surface.

inches; thicknesses ranged from 1 and 1/2 inches down to 3/64 inch. The actual sizes of specimens fabricated are shown as a matrix in Figure 3.4, eight gross volumes are tested.

To start this extended experimental activity, a bulk lot of 1045 steel was purchased. It came as a 4-inch diameter rod. This rod was cut up into 1-foot lengths for heat-treating. After these 1-foot sections are heat- treated to a "dead anneal" condition, as in the preliminary experiments, the 4-inch diameter is then reduced to either 1-inch or 2-inch as needed, or if a 4-inch specimen is required, the diameter is simply trued. Although time-consuming, this method of fabrication has the advantage that all specimens were made from the same stock of material, and also that the crack front in all specimens was at about the same location with respect to the original 4-inch diameter stock. After the proper specimen diameters were obtained, the specimen preparation was handled in a similar fashion to that of the preliminary experiments using scaled slitting saws as needed. The final fabrication step is grinding to final thickness.

Now, the specimens are fatigue-cracked to the same a/W value as the preliminary series. Fatigue pre-cracking proceeds as in the preliminary experiments except that it becomes more difficult to meet all the criteria of ASTM E399 since some are expressed in terms of absolute values; to wit, the minimum precrack is 0.05 inches [8]. A more important problem with the standard [8], is the application of ΔK to the precrack procedure involving various specimen sizes. When two specimens with different W's are precracked with the same ΔK, the smaller specimen experiences a larger $\Delta\sigma_n$, since $\Delta\sigma_n \propto \Delta K/\sqrt{W}$ for constant a/W. In an effort to minimize the strain-hardening experienced by the specimens before the actual fracture test, it is decided to use a minimum $\Delta\sigma_n$ in the crack growth procedure. All precracking was started at σ_n = 27 ksi and slowly increased until 97% of the desired crack growth could occur within several hundred thousand cycles. For the last 2 to 3% of crack growth the σ_n was reduced, meeting the intent of the ASTM standard [8].

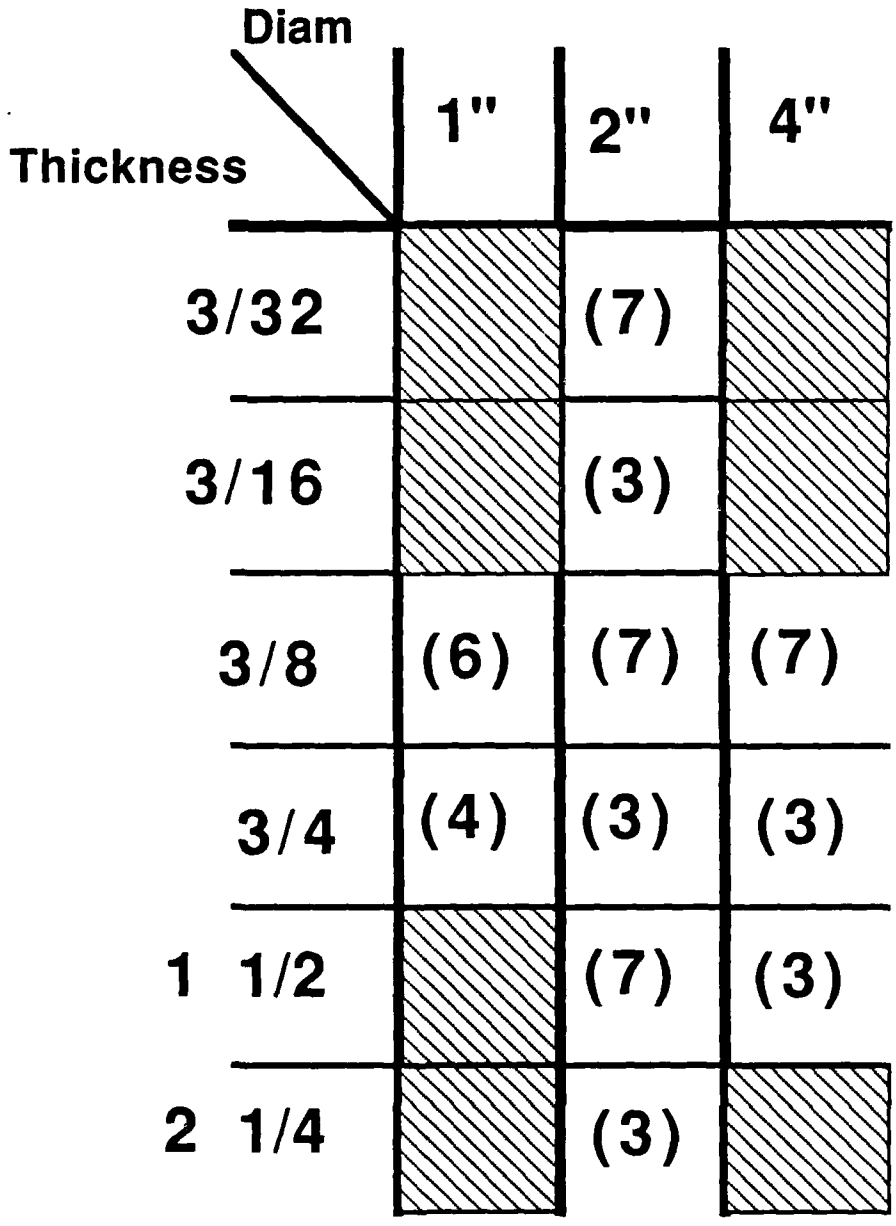

Figure 3.4 Matrix for extended experimental series.
(Numbers of specimens)

The order of fracture testing of the extended series of specimens is done in a somewhat random fashion so that trends in the data will not be associated with testing order. First a single specimen from a cross section of sizes is tested. Then, the testing can be thought of as going along by gross volumes. The eight gross volumes are collected into 3 groups by size, labeled large, middle and small, with 3, 3 and 2, respectively, volumes in the groups. The order of group testing then is: middle, large, small, middle, large, and finally, small. The actual liquid nitrogen fracture testing is done in a similar manner to that of the preliminary tests, as are the post-fracture measurements.

In addition, with this new stock, we repeat the tensile tests at liquid nitrogen temperatures. To accomplish this a heat-treated section is quartered and tensile specimens prepared along the lines of ASTM A 370 [140]. Four specimens, having diameters of either 0.35 or 0.175 inches, are prepared. They are tested in a liquid nitrogen bath, just as those of the preliminary series.

We are now in a position to present the results obtained for the extended experimental study, starting with the tensile tests. This time the specimens have between 4.6% and 2.6% reduction in area and ultimate strengths of 158.0 to 161.6 ksi. A typical stress-strain curve is shown in Figure 3.5. These results are comparable with data from MacGregor [141] for the same material, and seem to represent very brittle response.

The fractured specimens of this series, in general, are redolent of those of the preliminary study, having no shear lips and relatively flat fracture planes, with patent demarcation between areas of fatigue or precipitous cracking, see Plate 3.3. A typical load-displacement curve for a specimen in this series is rather similar to one of the preliminary study.

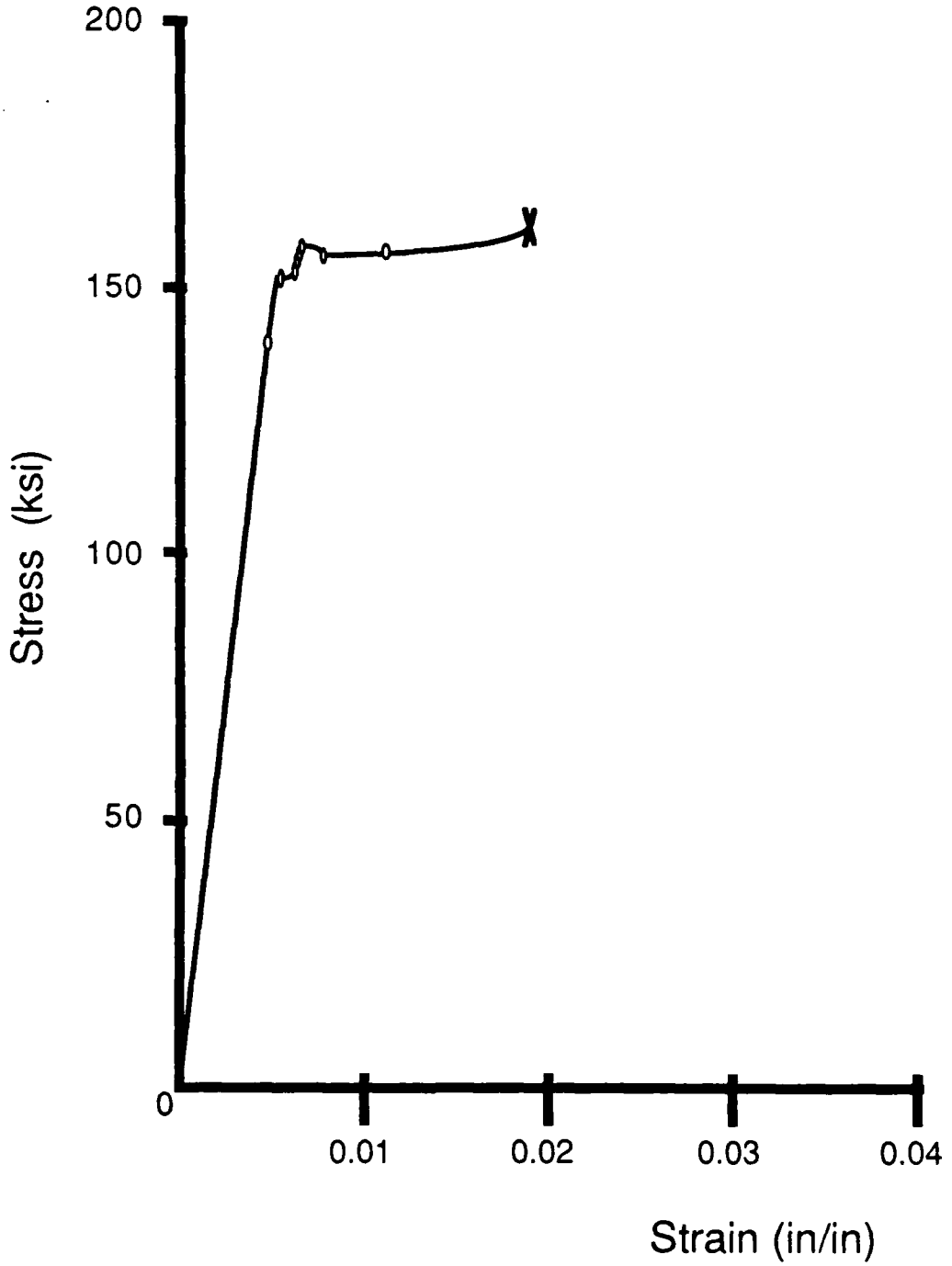

Figure 3.5 Typical stress strain curve for 1045 specimen tested in liquid nitrogen bath.

Plate 3.3 Fracture surface of specimen broken in liquid nitrogen bath.(4.8X)

Upon review of the results from this series, it is discovered that the curvature of the critical crack is more than anticipated, although not always enough to invalidate the test with respect to the standard [8]. As a result, many of the final raw a/W values are not within the closely confined region desired. To overcome this problem, it was decided that a weighted average be used with the results.

Upon examining the data further, a mean value of a/W of 0.553 seemed to include as many tests as possible. The actual procedure for weighting test results to arrive at this mean for each size is as follows. First the participation factor, f,is determined. This is done by setting f =1 when $0.540 \leq a/W \leq 0.566$, $0 < f < 1$ when $0.466 \leq a/W < 0.540$ or $0.566 < a/W \leq 0.640$ and such that the weighted mean equals 0.553, and f = 0 for other a/W. Under these rules there still remains some flexibility in choosing f; to reduce this we tried to pick f such that the maximum participation of test data occurred. The actual choice of f's lead to a sum of f's equal to 30.46, with some participation from 42 out of 53 specimens tested, and all sizes represented. With these f's, the average response for the specimen size is computed as the sum of the products of σ_n^* and f for each specimen, divided by the sum of the f's. (Details of results and participation factors are in Appendix C.)

For clarity, we first present the results in terms of thickness, or out-of-plane scaling. Figure 3.6 is a plot of normalized strength, σ_n^*, as in Figure 3.3, for each specimen of a given diameter, versus normalized thickness. The normalizing factors come from values of the largest thickness in each diameter. If the information of this figure were to follow the LEFM thickness prediction discussed in chapter 1, all the points should be along a horizontal line through 1.0, but they are not.

We now consider in-plane and out-of-plane scaling at once. To enable in-plane and out-of-plane size effects on strength, σ_n^*, to be plotted on a single graph, we use gross volume, as before. That is, we plot σ_N^* versus V as seen in Figure 3.7. As with the preliminary study, the

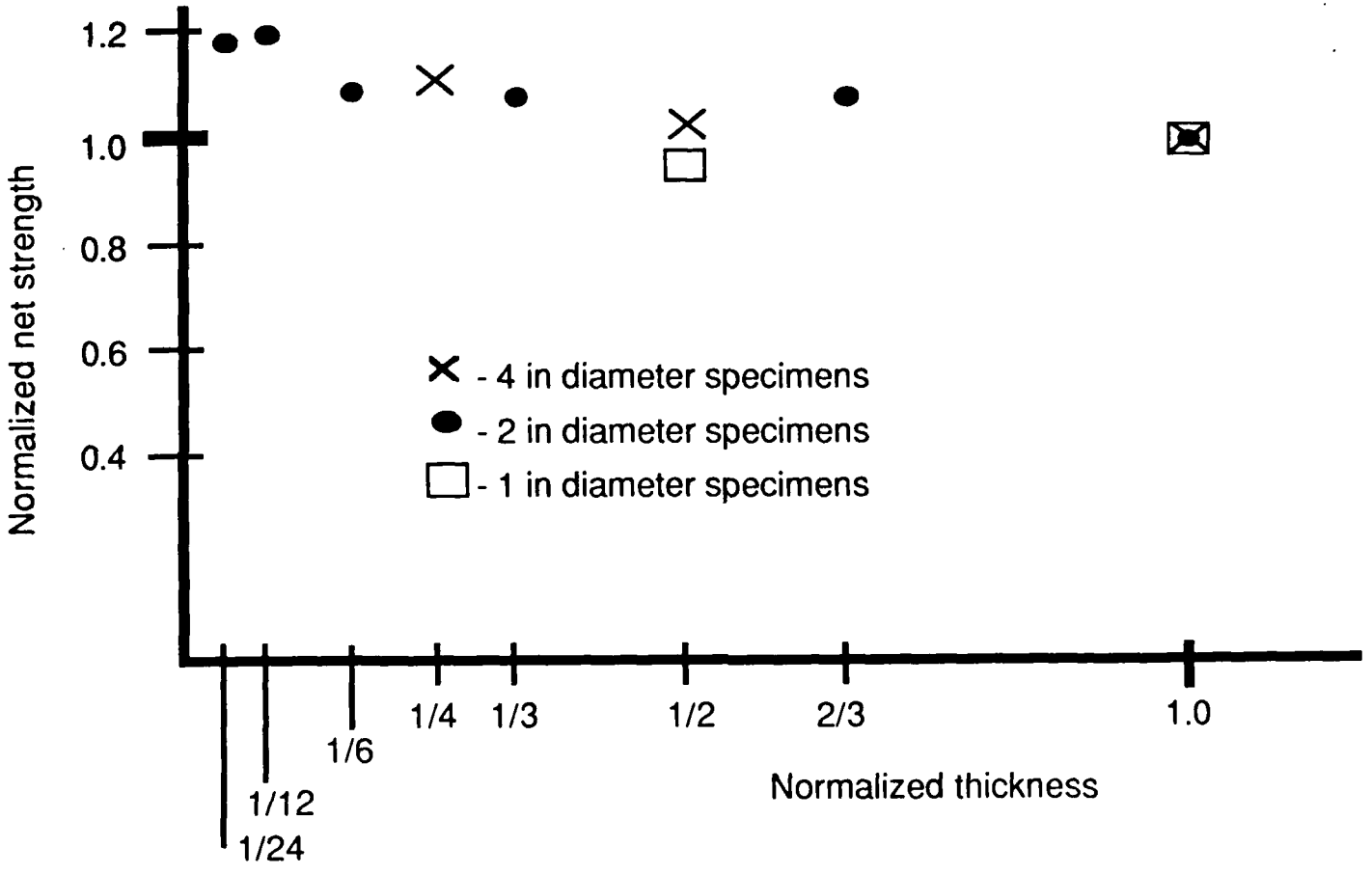

Figure 3.6 Plot of normalized net strength vs normalized thickness, extended study.

normalizing factor come from the largest specimen. Included with the stress values for each volume, are range bars for the results. In general, this figure portrays the type of behavior expected: that is as the specimen size gets small, the strength increases. This decrease in size is due to both in-plane and out-of-plane changes, the in-plane changes having the more pronounced effect.

Also shown in Figure 3.7, as the dotted line, is the prediction of strength based upon LEFM. The prediction uses the largest specimen as the starting point. The lines are flat since there is no thickness effected predicted. Note that as the specimens get smaller, the predictions get further off the mark, missing five of the eleven ranges entirely, and only getting the ranges for the smallest specimens because of the large amount of scatter involved. The mean error for the eleven predictions is 7% while the largest single error is an over prediction of about 16%. We can get a feeling for how well LEFM does with predicting the thickness effect alone by assuming LEFM predicts the σ_N^* of the largest gross volume in each planar set and looking at the resulting errors. The mean error for eight predictions is 10% and the largest single error is an under prediction of 19%.

The dashed line of Figure 3.7 represents a Weibull type plot [142], where the normalized stress is a function of the volume raised to some value, *i.e.* $\sigma_N^* = (V)^{\alpha}$. The value of the exponent, α, is selected as the one that best fits the experimental data in a least-squares fashion, weighted by the participation factor, here $\alpha = -0.1183$. This method does about the same as LEFM in that it misses the same number of ranges, and the average error is 0.08, and the worst single error is an under prediction of 20%.

Finally, the data is fitted to another model, as shown in the solid curve of Figure 3.7. This model represents the normalized strength as a function of a product of the in-plane scaling factor raised to a power and the out-of-plane factor raised to another; *i.e.* $\sigma_N^* = (W/W_0)^{\alpha} (B/B_0)^{\beta}$, where the 0 subscript indicates the normalizing value, or the value of the largest gross volume.

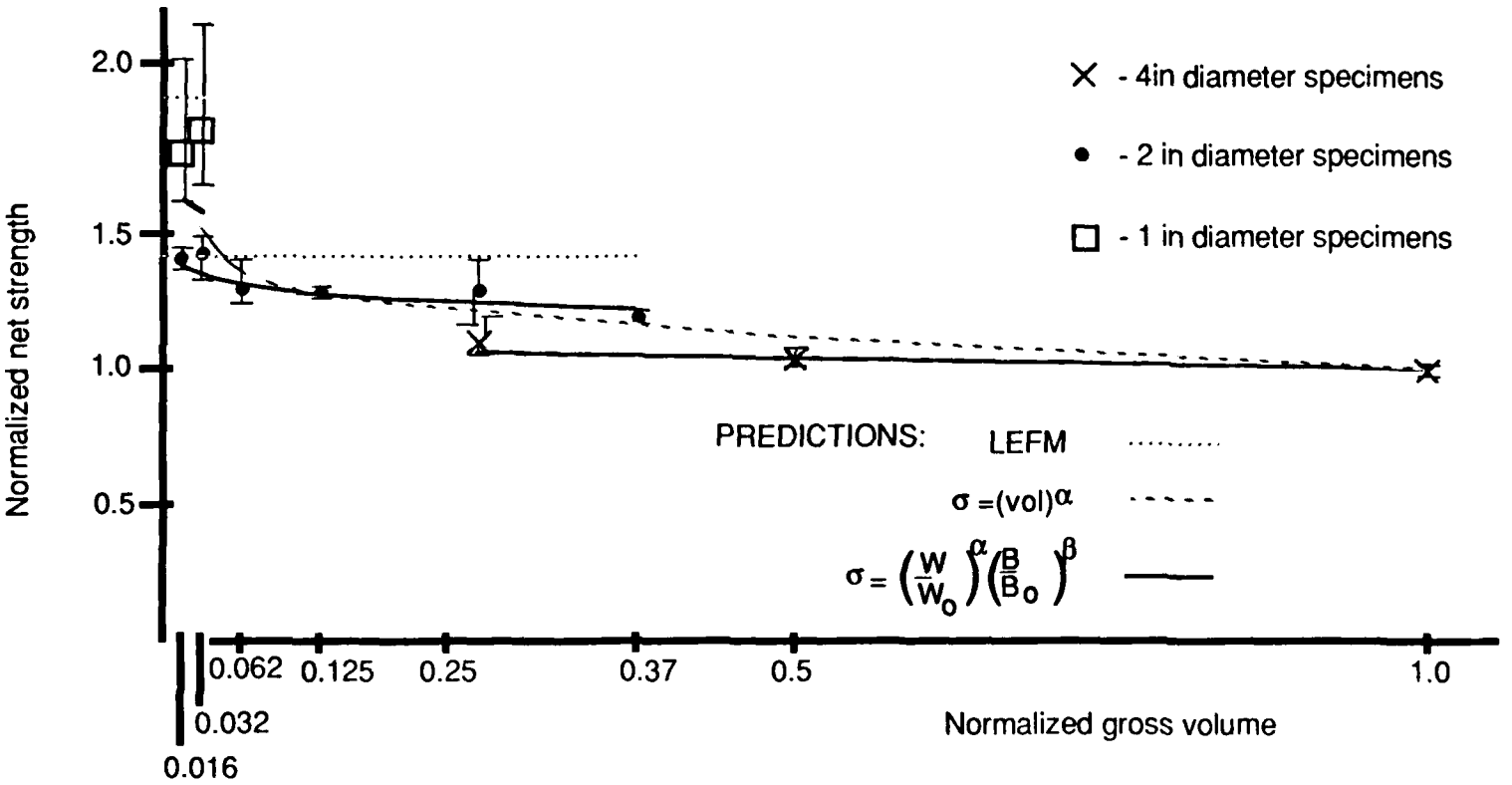

Figure 3.7 Plot of normalized net strength vs normalized gross volume, extended study.

The two exponents, α and β, are selected so as to hit as many data ranges as possible, here ten out of the eleven. Of the two exponents, α is largest, -0.31 versus -0.04 for β, and therefore has the larger impact on the strength. With these values, this model has a mean error of 5%, with the worst single error being a 16% under prediction. It is interesting to note that these two values are in the same trend as LEFM: that is to say -0.3 is not far from -0.5, and -0.04 is close to zero. A possible explanation for the success of this model is that the surfaces may be different from the interior by virtue of the machining they obtained.

4. CYCLIC LOADING EXPERIMENTS

Herein we describe a series of experiments whose primary objective is to be a pilot study on scaling effects in cyclic loading situations. We start this chapter by describing the experimental objectives. This is followed by a description of how the specimens are prepared and the experiments conducted. We conclude the chapter by discussing the data reduction methods used and results found.

The primary objective of this experimental series is to conduct a pilot study into the scaling effects in a cyclic loading situation, and see how consistent these results are with LEFM. We chose to look at the complete scaled situation, *i.e.* proportional changes in length and thickness as well as width, as shown in Figure 1.3. We attempt to isolate other factors by doing the following: using the same material, cycling at the same frequency, conducting the tests at the same temperature, applying a constant stress amplitude in all tests, and employing the same R ratio, where R is the minimum cyclic stress divided by maximum cyclic stress. As with the monotonic experiments, we wish to control scatter and therefore will use several specimens in each size. Also, we attempt to comply with ASTM standards, namely E 647 [143] because of their general acceptance within the fracture mechanics community.

The experiments use center-cracked panels scaled with respect to width, thickness and length by a factor of four, a factor of four being the largest compatible with the test rig and machining practices, Figure 4.1. Detailed preparation of the specimens is in accordance with ASTM Standard E 647 [143]. The center starter crack is machined into the material using a wedge-shaped flycutter. The result of this is that the both ends of the crack have a chevron starter area. This method of producing the center crack is scaled for both sizes, *i.e.*, an exactly 1/4-size flycutter is used to cut the smaller specimen. During the fabrication, the specimens are all aligned in such a manner that the rolling direction is the same with respect to the center crack. The next step in the preparation is to measure the specimens and the center-crack geometry

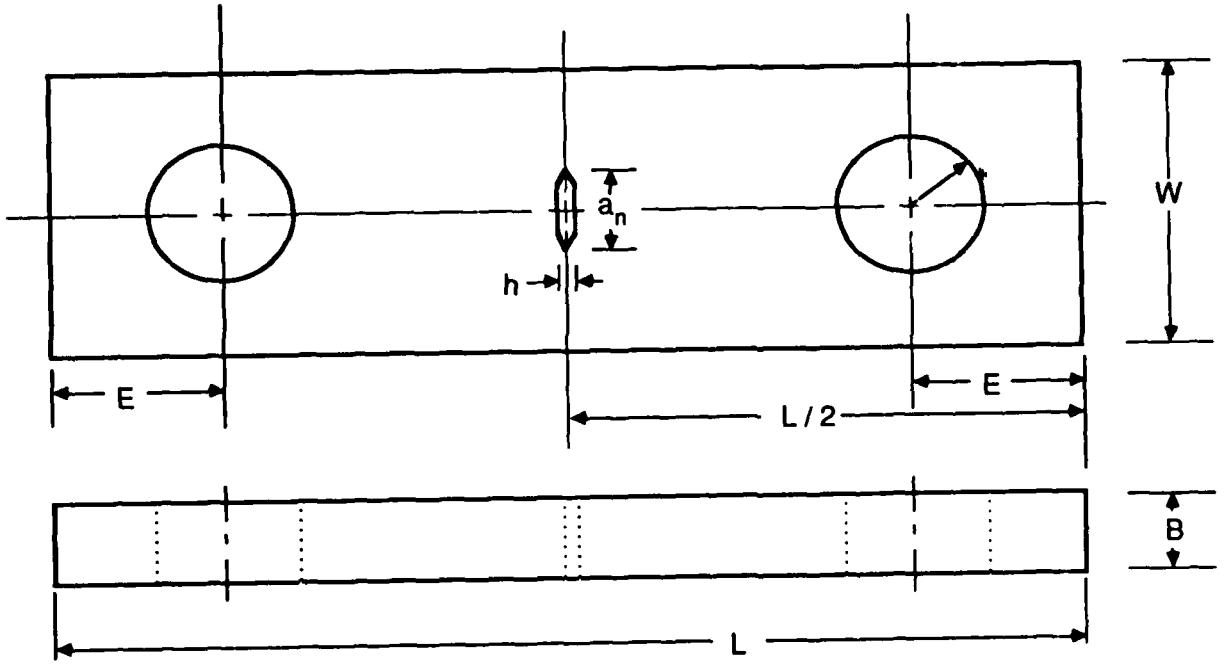

Dimension (in)	Lg.	Sm.
W	3.0	0.75
L	12.0	3.0
B	1/8	1/32
a	1.0	0.25
h	3/16	0.047
E	1.5	3/8
r	0.5	1/8

Figure 4.1 Specimen, and typical dimensions, used for cyclic experiments.

completely. Inspection microscopes are used for this operation. The specimens are made of aluminum 2024-T3 in contrast to the steel of the monotonic loading experiments. Loading for both specimen sizes is at the same frequency (20 Hz), with an R-ratio of 0.1, and applied stress variation, $\Delta\sigma$, equal to 9.6 ksi. Testing is carried out on sets of six specimens of each size, six being the minimum deemed necessary to gauge scatter.

The execution of the experiments tried to follow the guidelines set forth in ASTM E 647 [143]. The experiments are conducted on a typical MTS 22 Kip servo-hydraulic feedback testing machine. The test set-up is shown in Plate 4.1. The order of testing is such that some large specimens are tested, then smaller specimens, finally finishing with the remainder of the large specimens. This is done to limit any systemic trend in the data due to testing sequence. Another aspect of the experimental procedure is the measurement of the crack during cycling. To accomplish this, an optical method is used. This consists of a strobe light synchronized to the maximum load signal of the machine and a traveling microscope. The operational details of this setup are that the measurements are taken only from the front surface and that the left and right sides of the crack are alternately measured. Since a strobe is used, there is no need to halt the machine operation for measurement. The experiments then continued until fracture. Cycles to fracture, N, are recorded as well as the crack length before catastrophic failure, a_f. (A summary of the raw test data for all specimens is contained in Appendix C.)

The next step is to do the data reduction. This starts by combining the left and right side measurements for a specimen. Incorporated in this combining is the implicit assumption that crack growth is symmetric, being hopefully justified by the efforts to ensure symmetry. The ASTM standard [143] presents two possible ways for data reduction. These two methods are the secant method and the seven -point polynomial method. Both were applied to the data.

Individual results in the form of points on a da/dN versus ΔK plot are shown in Figure 4.2. This figure superimposes the results for all specimens in the two sizes. Viewing this figure, one

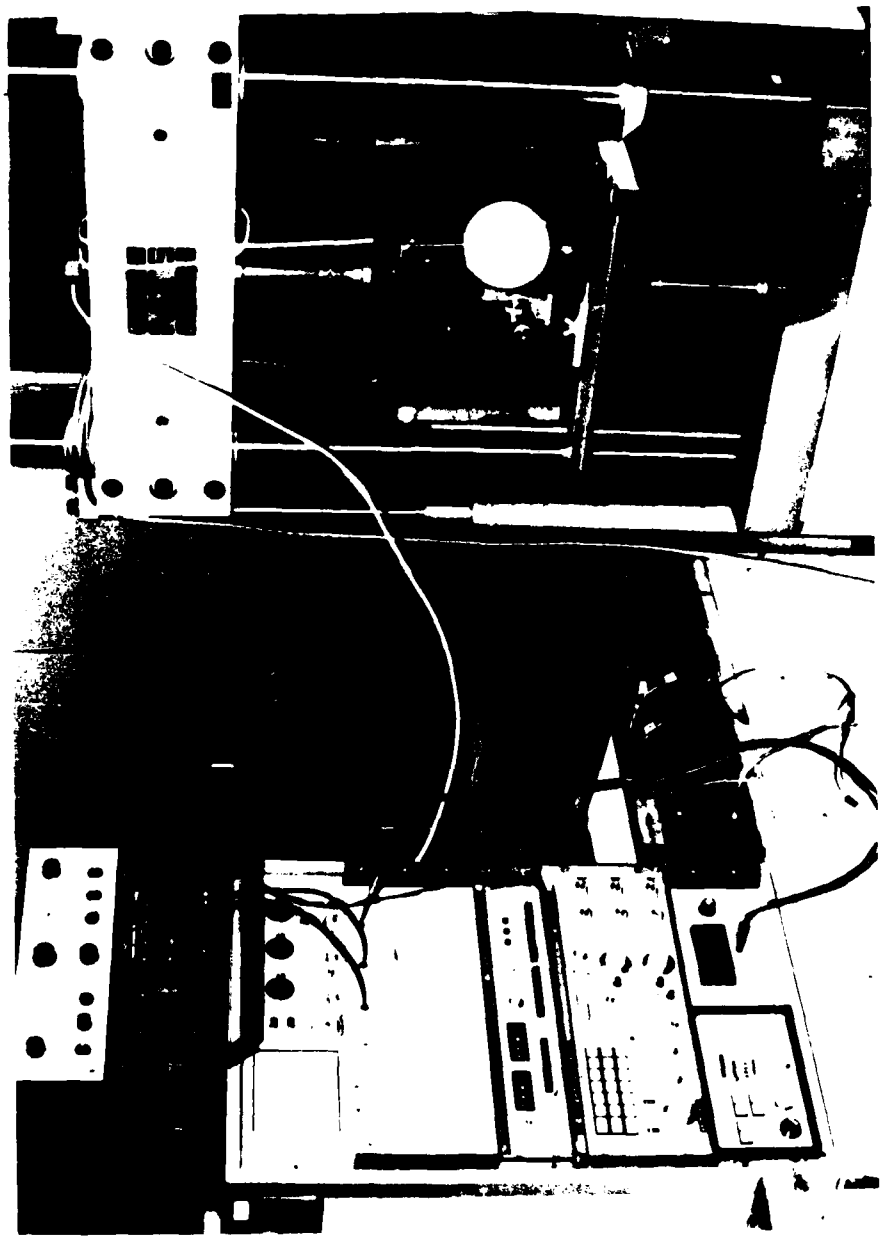

Plate 4.1 Equiptment set-up for the cyclic experiments.

notes the typical three-stage shape of the two superimposed curves. Although the center linear portions of the two curves are roughly parallel, it is important to note that the initial and final stages of the two curves have a relatively large offset. The Paris parameters of (1.4), obtained from a least-squares fit to the data, are shown in Table 4.1. Both Figure 4.2 and the results in Table 4.1 essentially remain the same whether the secant method or the seven-point polynomial method is used.

The first thing to note concerning the values in Table 4.1, is that it would not appear reasonable to attribute the changes in m, or C with size to scatter alone, since neither the mean m nor the mean C for one size lies within the corresponding range for m, or C of the other. Indeed, the ranges themselves for m and C overlap less than 16% and 24% of their combined extents, respectively. It thus seems likely that these results demonstrate that m and C can exhibit significant dependence on size. Furthermore, the end points of the validity of the data fits are size dependent. Hence if one were estimating what would occur in a small specimen using the data from the big when crack propagation started at a ΔK of, say, 13, one one might be inclined to predict indefinite life, or at least to predict it lasting as many cycles as the larger specimens typically survived - here, on average, 27,000. In fact, the smaller specimens only lasted an average of 4,000 cycles from this point. While it is now generally recognized that the notion of a threshold ΔK as a material property is invalid, this example does serve notice of the dangers of regarding either ΔK_{min} or ΔK_{max} as a size-independent material constant† . In all, then, for the present set of experiments, cyclic life predictions based on the Paris data reduction scheme may be unacceptably unreliable.

---

† Such a potentially dangerous interpretation is implicit in the sinh fit of Annis, Wallace, and Sims [144].

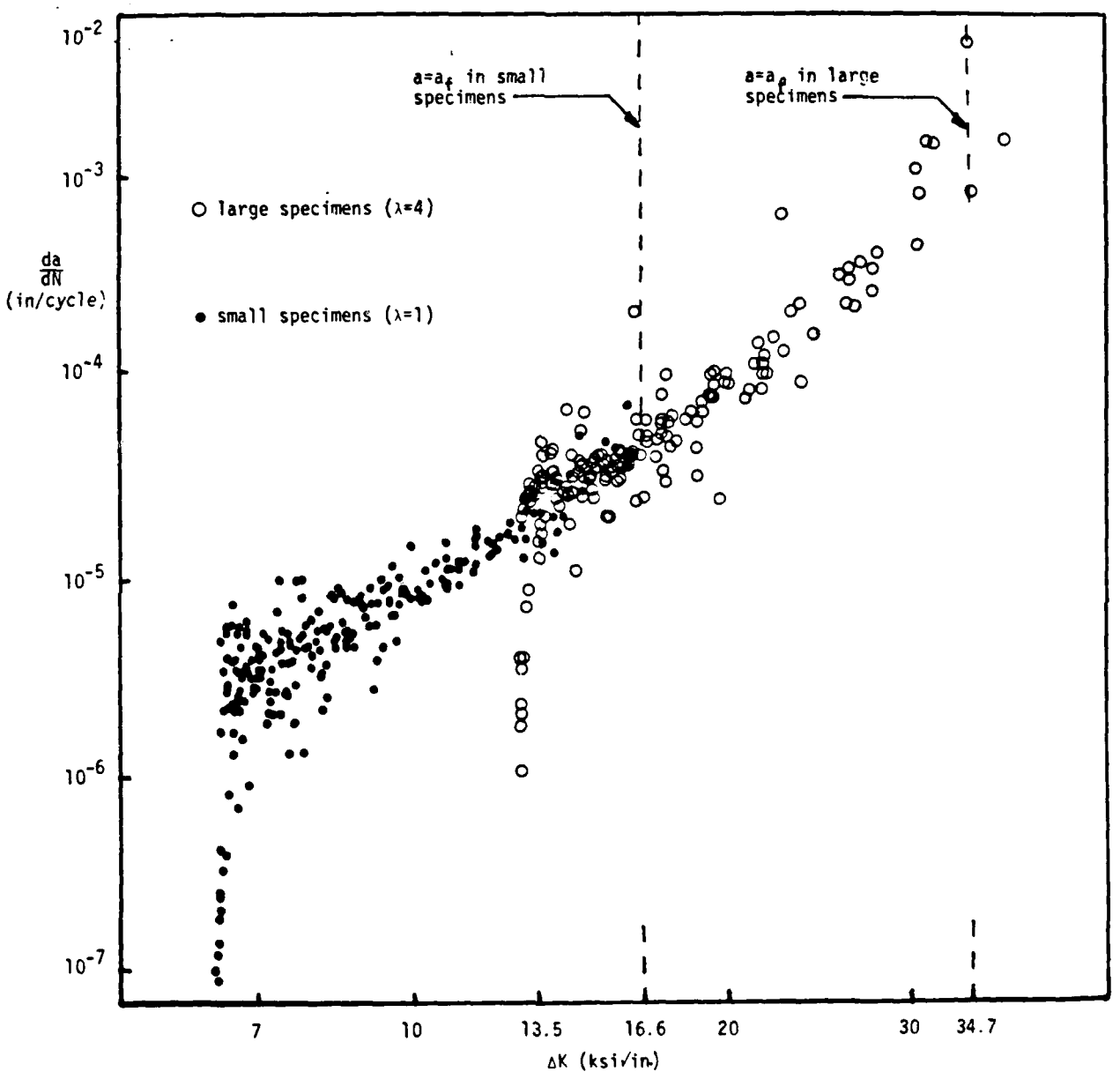

Figure 4.2 Crack growth rates versus ΔK.

Finally, here we check the size dependence given earlier, namely,

$$\frac{N^*_S}{N^*_I} = \lambda^{(m/2\ -1)} \qquad (4.1)$$

We evaluate (4.1) with the data of Table 4.1, using m from both sizes. The predicted value of (4.1), using m from the small and large specimens is 1.66 and 2.36, respectively. The ratio of actual average N^*_S to actual average N^*_I is 2.93. So neither represents very good agreement.

Table 4.1 Parameters obtained from cyclic experiments.

Quantity	Small specimens (λ=1)	Large Specimens (λ=4)
m, mean	2.73	3.24
m, range	2.59-3.03	2.88-3.54
C, mean ($x10^{10}$)	173	65.4
C,range ($x10^{10}$)	91-228	20-140
N, mean ($x10^3$)	27.4	80.2
ΔK_{min} (ksi$\sqrt{in}$)	6.9	13.5
ΔK_{max} (ksi$\sqrt{in}$)	14.1	30.2

5. CONCLUDING REMARKS

In this final chapter, we attempt to summarize the information contained in the preceding chapters and discuss its implications for LEFM. We begin by looking at the three particular scaling situations in question and review the information obtained from both literature and experimental studies in each situation. We continue by expressing some thoughts on the consequences of this information for LEFM, and conclude by discussing possible areas of further activities.

We first address the situation of in-plane scaling for monotonically-loaded specimens. As expressed in Chapter 2, the summary of literature review by Sinclair and Chambers [7] indicates that reported data do not agree well with the square-root scaling prediction of LEFM see (1.3), as shown in Figure 2.1. The prediction becomes further removed from the data as the scaling factor increases, tending to over predict the strength in smaller specimens. The experimental results described in Chapter 3 also showed a failure to predict strength changes with scaling. However, in these experiments, the overestimate occurred as the specimens got smaller, and the inaccuracies were not as pronounced as for some of the data found in [7]. Nonetheless, in all LEFM's performance in this regard is less than satisfactory.

Next, we turn our attention to the out-of-plane scaled situation. The literature review in this area indicates that there is no definitive trend to the reported data. In fairness, it should be pointed out that these data represent a limited number of experiments, at least for brittle materials, and which typically did not have large scaling factors. The experiments reported upon in Chapter 3 exhibited a strength variation with out-of-plane scaling. Figure 3.7 shows that the out-of-plane scaling effect does not have as pronounced an impact on the normalized strength as does the in-plane effects. For this case, the "flat line" prediction of LEFM is conservative and underestimates the strength increase. However, because of the limited ductility of the material in the test conditions, it is clear that no explanation which is based solely on a material ductility aspect could

fully explain this situation. In all, the understanding of thickness effects in LEFM is less than complete.

To quantify the above situation for in-plane and out-of-plane scaling, consider the expression $\sigma_N^* = \lambda^\alpha$, and the changes in σ_N^* as a result of setting α to either 0.3 or 0.5. We construct a ratio of $\lambda^{0.3}/\lambda^{0.5}$, and note how this ratio varies with the scaling factor, λ. For $\lambda = 2$, the ratio is 1.23/1.41, or 0.87, indicating about a 13% difference in predicted strength. As λ is increased, the ratio changes, such that when $\lambda = 8$, the ratio is 1.87/2.83, or 0.66. If λ gets up to 16, the ratio becomes 0.57. Clearly the impact of α is dependent upon the scaling factor; if λ is large, large differences in strength predictions result from small variations in λ. However, for out-of-plane scaling, with α being either0.0 or 0.04, the above ratio will only vary by 12% even for a scaling of 20.

Finally we address the last question under study, we consider scaling effects in cyclically-loaded situations. The literature review in this area was most noteworthy for its relatively few reports. These contributions seem to question the validity of assuming the invariability of the material parameters, C and m, of the Paris Law, (1.4). In using such reports to determine the effect of scaling on lifetime predictions, there seems to be no clear trend. Sometimes the data indicates increases in lifetime, while, in other cases, decreases in lifetime. Also noteworthy in these contributions is the lack of information about behavior of the range of applicability with scaling. The reported experimental results of Chapter 4 raised similar questions about C and m and the ability to predict lifetimes. However, what may be of more important consideration is that these experiments indicated a possible shift of the range of applicability. This could imply a finite life for items believed to be designed within "infinite life" parameters. In sum, the LEFM treatment of cyclic life prediction for scaled specimens appears to be potentially quite unreliable.

Overall, LEFM is trendwise generally correct in its predictions of size effects, but so oversimplified that it is unreliable as an engineering technology. It seems that what ever size

effects are present for a given material, LEFM does not usually predict them accurately enough. This is probably because these effects are dependent upon the microstructure of the material under consideration and LEFM, being based on the continuum mechanics of homogeneous materials, does not include the effects of microstructure. In order to accommodate size effects, therefore, microstructure will need to be incorporated. Just how this should be done is a challenging question, one which is beyond the scope of the present work. However, it seems fairly certain that such a question will have to be considered by future workers if we are to arrive at a more reliable technology.

REFERENCES

1 M.F. Kanninen, and C.H. Popelar, *Advanced Fracture Mechanics*, Oxford University Press, New York (1985).

2 J. J. Duga, W. H. Fisher, R. W. Baxhaum, A. A. Rosenfield, A. R. Buhr, E.J. Hourton, and S. C. McMillan, "Fracture Costs US $119 Billion a Year, Says Study by Battelle/NBS", *International Journal of Fracture*, 23 (1983) R81-R83.

3 J. J. Duga, W. H. Fisher, R. W. Baxhaum, A. A. Rosenfield, A. R. Buhr, E.J. Hourton, and S. C. McMillan, "The Economic Effects of Fracture in the United States, Pt2,- A Report to NBS by Battelle Columbus Laboratories", *U.S. Deptartment of Commerce, NBS Special Publication* 6.47-2, 1983.

4 S. T. Rolfe and J.M. Barsom, *Fracture and Fatigue Control in Structures, Application of Fracture Mechanics*, Prentice-Hall, Inc., Englewood Cliffs, N.J., (1977).

5 D. Broek, *Elementry Engineering Fracture Mechanics, 3rd Ed.*, Martinus Nijhoff, Boston, (1982).

6 K.E. Puttick and A. G. Atkins, "The Scaling laws of Stage II Fatigue Fracture", *International Journal of Fracture*, 23 (1983) R51-R54.

7 G. B. Sinclair and A. E. Chambers, "Strength Size Effects and Fracture Mechanics: What Does the Physical Evidence Say?", *Engineering Fracture Mechanics*, 26 (1987) 279-310.

8 1985 Annual Book of ASTM Standards, Vol. 03.01, *American Society for Testing and Materials*, Philadelphia, (1985) 547-582.

9 W. R. Andrews, V. Kumar, and M. M. Little, "Small-Specimen Brittle-Fracture Toughness Testing", *Fracture Mechanics: Thirteenth Conference, ASTM STP 743* (1981) 576-598.

10 S. N. Bandyopadhyay, N. Singh and G. S. Murty, "An Experimental Study of Crack Tip Plastic Flow in Mild Steel", *Engineering Fracture Mechanics*, 14 (1981) 565-580.

11 S. Banerjee, "Influence of Specimen Size and Configuration on the Plastic Zone Size, Toughness and Crack Growth", *Engineering Fracture Mechanics*, 15 (1981) 343-390.

12 J. T. Barnby and I. S. Al-Daimalani, "Assessment of the Fracture Toughness of Cast Steels, Part 1, Low Alloy Steels", *Journal of Materials Science*, 11 (1976) 1979-1988.

13 J. T. Barnby and I. S. Al-Daimalani, "Assessment of the Fracture Toughness of Cast Steels, Part 2, Carbon and Carbon Manganese Steel" , *Journal of Materials Science*, 11 (1976) 1989-1994.

14 C. Bathias, "Application of Fracture Mechanics to Aluminum Alloys Selection", *Engineering Fracture Mechanics*, 10 (1978) 267-282.

15 A. D. Batte, W. S. Blackburn, A. Elsender, T. K. Hellen, and A. D. Jackson, "A Comparison of the J* Integral with Other Methods of Post Yield Fracture Mechanics", *International Journal of Fracture*, 21 (1983) 49-66.

16 J. C. Behiri and W. Bonfield, "Fracture Mechanics of Bone–The Effects of Density, Specimen Thickness and Crack Velocity on Longitudinal Fracture", *Journal of Biomechanics,* 17, No. 1 (1984) 25-34.

17 M. W. Birch, M. D. Taylor and G. P. Marshall, "Design for toughness in polymers. 4 - The Effect of Geometry on Stable Crack Propagation in the Thermoplastics for Pressure Pipe Duties", *Plastics and Rubber Processing and Applications,* 3 (1983) 281-291.

18 W. F. Brown, Jr. and J. E. Srawley, "Plane Strain Crack Toughness Testing of High Strength Metallic Materials", *ASTM Special Technical Publication No. 410* (1966) 1-65.

19 M. K. V. Chan and J. G. Williams, "Plane Strain Fracture Toughness Testing of High Density Polyethylene", *Polymer Engineering and Science,* 21 (1981) 1019-1026.

20 G. G. Chell and P. J. Worthington, "The Determination of Fracture Toughness of a Tough Steel from Invalid Compact Tension Specimens of Varying Width and Thickness", *Materials Science and Engineering,* 26 (1976) 95-103.

21 A. Elsender, A. Poynton and D. Batte as reported in G. G. Chell, and R. S. Gates, "A Study of Failure in the Post Yield Regime Using Single Edge-Notched Tension Specimens", *International Journal of Fracture,* 14 (1978) 233-247.

22 A. Frediani, "An Evaluation of the Reliability of Fracture Mechanics Methods", *Engineering Fracture Mechanics,* 14 (1981) 289-322.

23 J. Fukakura, "The Effect of Specimen Thickness and Temperature on Plastic Yielding and Fracture Properties of Mild Steel", *Engineering Fracture Mechanics,* 6 (1974) 231-244.

24 K. S. Grewal and V. Weiss, "The Effect of Testing System Stiffness on Fracture Behavior of Sheet Specimens", *Proceedings of the Second Int.ernational Conference on Fracture,* Brighton, U.K., (1969) 94-104.

25 C. A. Griffis, "Elastic-Plastic Fracture Toughness: A Comparison of *J*-Integral and Crack Opening Displacement Characterizations", *Journal of Pressure Vessel Technology, Transactions of the ASME,* Nov. (1975) 278-283.

26 R. H. Heyer and D. E. McCabe, "Crack Growth Resistance in Plane-Stress Fracture Testing", *Engineering Fracture Mechanics,* 4 (1972) 413-430.

27 T. Hollstein, W. Schmitt, and J. G. Blauel, "Numerical Analysis of Ductile Fracture Experiments Using Single-Edge Notched Tension Specimens", *Journal of Testing and Evaluation,* 11 (1983) 174-181.

28 F. H. Huang and D. S. Gelles, "Influence of Specimen Size and Microstructure on the Fracture Toughness of a Martensitic Stainless Steel", *Engineering Fracture Mechanics,* 19 (1984) 1-20.

29 C. M. Hudson and P. E. Lewis, "NASA-Langley Research Center's Participation in a Round-Robin Comparison Between Some Current Crack-Propagation Prediction Methods", *Part-Through Crack Fatigue Life Prediction, ASTM STP 687,* (1979) 113-128.

30 G. R. Irwin, J. A. Kies, and H. L. Smith, "Fracture Strengths Relative to Onset and Arrest of Crack Propagation", *Proceedings of the American Society for Testing and Material,* 58 (1958) 640-657.

31 W. S. Johnson, "Damage Tolerance Evaluation of Adhesively Laminated Titanium", *Journal of Engineering Materials and Technology, Transactions of the ASME*,105 (1983) 182-187.

32 M. H. Jones and W. F. Brown, Jr., "The Influence of Crack Length and Thickness in Plane Strain Fracture Toughness Tests", *Review of Developments in Plane Strain Fracture Toughness Testing, ASTM STP 463*, (1970) 63-101.

33 H.-J. Kaiser and K. E. Hagedorn, "A Comparison of Different Methods for Determination of Elastic-Plastic R-Curves", *Proceedings ofThird Colloquium on Fracture*, London, U.K., (1980) 79-86.

34 J. G. Kaufman, "Discussion", *Fracture Toughtness Testing and Its Application, ASTM STP 381* (1965) 208-209.

35 J. G. Kaufman, "Progress in Fracture Testing of Metallic Materials", *Review of Developments in Plane Strain Fracture Toughness Testing ASTM STP 463* (1970) 3-21.

36 J. S. Ke and H. W. Liu, "Thickness Effect on Crack Tip Deformation at Fracture", *Engineering Fracture Mechanics*, 8 (1976) 425-436.

37 A. J. Kinloch and R. A. Gledhill, "Propellant Failure: A Fracture-Mechanics Approach", *Journal of Spacecraft*, 18 (1981) 333-337.

38 J. F. Knott, Discussion, *Proceedings of the Royal Society of London, Series A.*, 285 (1965) 150-159.

39 H. Liebowitz, J. Eftis, and D. L. Jones, "Some Recent Theoretical and Experimental Developments in Fracture Mechanics", *Fracture 1977*, 1 (1977) 695-723.

40 S. Mindess and J. S. Nadeau, " Effect of Notch Width on K_{IC} for Mortar and Concrete", *Cement and Concrete Research*, 6 (1976) 529-534.

41 E. M. Morozov, "Some Problems in Experimental Fracture Mechanics", *Engineering Fracture Mechanics*, 13 (1979) 541-561.

42 D. F. Mowbray, A. J. Brothers, and S. Yukawa, "Fracture Toughness Determinations of A-302B and Ni-Mo-V Steels with Various Size Specimens", *Journal of Basic Engineering,Transactions of the ASME*, December (1966) 783-791.

43 D. Munz and H. P. Keller, "Effect of Specimen Size on Fracture Toughness in the Ductile Brittle Transition Region of Steel", *Proceedings of the Third Colloquium on Fracture, London, U.K.*, (1980) 105-117.

44 B. K. Neale, "An Investigation into the Effect of Thickness on the Fracture Behaviour of Compact Tension Specimens", *International Journal of Fracture*, 14, No. 2 (1978) 203-212.

45 S. P. Petrie, A. T. DiBenedetto, and J. Miltz, "The Effects of Stress Cracking on the Fracture Toughness of Polycarbonate", *Polymer Engineering and Science*, 20, No. 6 (1980) 385-392.

46 L. P. Pook, " Fracture Toughness Tests on an Aluminium Alloy Using a Chevron Notch Bend Specimen", *International Journal of Fracture* , 22 (1983) R21-R23.

47 P. K. Poulose, D. L. Jones, and H. Liebowitz, "A Comparison of the Geometry Dependence of Several Nonlinear Fracture Toughness Parameters", *Engineering Fracture Mechanics,* 17, No. 2 (1983)133-151.

48 S. K. Putatunda and S. Banerjee, "Effect of Size on Plasticity and Fracture Toughness", *Engineering Fracture Mechanics,* 19 (1984) 507-529.

49 D. T. Read and R. P. Reed, "Effects of Specimen Thickness on Fracture Toughness of an Aluminum Alloy", *Internation Journal of Fracture,* 13, No. 2 (1977) 201-213.

50 A. J. Repko, M. H. Jones, and W. F. Brown, Jr., "Influence of Sheet Thickness on Sharp-Edge-Notch Properties of a β Titanium Alloy at Room and Low Temperatures", *Symposium on Metallic Materials for Low-Temperature Service, ASTM STP 302,* (1961) 213-229.

51 P. C. Riccardella and J. L. Swedlow, "A Combined Analytical-Experimental Fracture Study", *Fracture Analysis ASTM STP 560,* (1974) 134-154.

52 S. T Rolfe and S. R. Novak, Discussion, *Review of Developments in Plane Strain Fracture Toughness Testing, ASTM STP 463,* (1970) 63-101.

53 R. A. Schmidt and T. J. Lutz, "K_{IC} and J_{IC} of Westerly Granite - Effects of Thickness and In-Plane Dimensions", *Fracture Mechanics Applied to Brittle Materials, ASTM STP 678* (1979)166-182.

54 J. L. Shannon, Jr., J. K Donald, and W. F. Brown, Jr., "Heavy-Section Fracture Toughness Screening Specimen", *Developments in Fracture Mechanics Test Methods Standardization, ASTM STP 632* (1977) 96-114.

55 J. L. Sliney, Jr., "Notch Properties of 5 Per Cent Chromium-Molybdenum-Vanadium Steel Sheet as Affected by Heat Treatment, Test Temperature, and Thickness", *Proceedings of the Americam Society for Testing and Materials,* 62 (1962) 825-836.

56 D. G. Smith and M. Chowdary, "The Fracture Toughness of Slip-Cast Fused Silica", *Materials Science and Engineering,* 20 (1975) 83-88.

57 J. E. Srawley and C. D. Beachem, "Resistance to Crack Propagation of High-Strength Sheet Materials for Rocket Motor Casings", *NRL Technical Report No. WAL TR 310.24/4,* (1962) 1-54.

58 E. A. Steigerwald, "Crack Toughness Measurements of High-Strength Steels", *Review of Developments in Plane Strain Fracture Toughness Testingf, ASTM STP 463* (1970) 102-123.

59 E. A. Steigerwald and G. L. Hanna, "Initiation of Slow Crack Propagation in High-Strength Materials", *Proceedings of American Society for Testing and Materials,* 62 (1962) 885-913.

60 A. M. Sullivan and J. Stoop, "Further Aspects of Fracture Resistance Measurement on Thin Sheet Material: Yield Stress and Crack Length", *Fracture Toughness and Slow-Stable Cracking, ASTM STP 559* (1974) 99-110.

61 A. M. Sullivan, J. Stoop, and C. N. Freed, "Influence of Sheet Thickness Upon the Fracture Resistance of Structural Aluminum Alloys", *Progress in Flaw Growth and Fracture Toughness Testing, ASTM STP 536* (1973) 323-333.

62 S. Taira and K. Tanaka, "Thickness Effect of Notched Metal Sheets on Deformation and Fracture under Tension", *Engineering Fracture Mechanics*, 11(1979) 231-249.

63 D. N. Williams, "Effect of Specimen Thickness on Subcritical Crack Growth under Sustained Load", *Materials Science and Engineering*, 18 (1975) 149-155.

64 J. G. Williams and P. D. Ewing, "Crack Propagation in Plates and Shells Subjected to Bending and Direct Loading", *Proceedings of the Second International Conference on Fracture*, Brighton, U.K., (1969) 119-130.

65 D. H. Winne and B. M. Wundt, "Application of the Griffith-Irwin Theory of Crack Propagation to the Bursting Behavior of Disks, Including Analytical and Experimental Studies", *Transactions of the ASME*, 80 (1958) 1643-1655.

66 S. Yukawa, "Testing and Design Considerations in Brittle Fracture", *Symposium on Evaluation of Metallic Materials in Design for Low-Temperature Service, ASTM STP 302* (1961) 193-212.

67 R. E. Zinkham, "Anisotropy and Thickness Effects in Fracture of 7075-T6 and -T651 Aluminum Alloy", *Engineering Fracture Mechanics*, 1 (1968) 275-289.

68 S. Banerjee, "A New Approach to Fracture Mechanics Based Testing and Analysis", *Metallurgical Engineer - I.I.T., Bombay*, 12 (1981) 5-10.

69 J. D. Barrett, "Effect of Crack-Front Width on Fracture Toughness of Douglas-Fir", *Engineering Fracture Mechanics*, 8 (1976) 711-717.

70 J. M. Barsom and S. T. Rolfe, "K_{IC} Transition-Temperature Behavior of A517-F Steel", *Engineering Fracture Mechanics*, 2 (1971) 341-357.

71 J. A. Begley and J. D. Landes, "The *J* Integral as a Fracture Criterion", *Fracture Toughness, Proceedings of the 1971 National Symposium on Fracture Mechanics, Part II, ASTM STP 514* (1972) 1-20.

72 D. R. Biswas and V. K. Pujari, "Verification of the Double-Torsion Equation by Using Different Thickness Samples of a Machinable Glass-Ceramic", *Communications of the American Ceramic Society*, July (1981) 98-99.

73 J. M. Bloom, "Validation of a Deformation Plasticity Failure Assessment Diagram Approach to Flaw Evaluation",*Elastic-Plastic Fracture: Second Symposium, Vol. II - Fracture Resistance Curves and Engineering Applications, ASTM STP 803*, (1983) II-206-II-238.

74 J. I. Bluhm, " A Model for the Effect of Thickness on Fracture Toughness", *Proceedings of the American Society for Testing and Materials*, 61 (1961)1324-1331.

75 S. W. J. Boatright and G. G. Garrett, "The Effect of Microstructure and Stress State on the Fracture Behaviour of Wood", *Journal of Materials Science*, 18 (1983) 2181-2199.

76 R. M. Bruscato, "The Measurement of Crack Arrest Fracture Toughness in Welded 9% Nickel Steels Used in Cryogenic Storage Tanks", *Welding Research, Supplement to the Welding Journal*, July (1981) 113-s -120-s.

77 F. E. Buresch, "Fracture Toughness Testing of Alumina", *Fracture Mechanics Applied to Brittle Materials, ASTM STP 678* (1979) 151-165.

78 G. G. Chell and A. Davidson, "A Post-Yield Mechanics Anaylsis of Single Edge Notched Tension Specimens", *Materials Science and Engineering*, 24 (1976) 45-52.

79 G. G. Chell and I. Milne, "A New Approach to the Analysis of Invalid Fracture Toughness Data", *International Journal of Fracture*, 12 (1976) 164-167.

80 E. P. Cox and F. V. Lawrence, Jr., "Ductile Fracture Behavior of Wrought Steels", *Fracture Mechanics: Twelfth Conference, ASTM STP 700*, (1980) 529-551.

81 K. Endo, K. Komai, and I. Yamamoto, "Effects of Specimen Thickness on Stress Corrosion Cracking and Corrosion Fatigue of An Aluminum Alloy", *Bulletin of the JSME*, 24, No. 194 (1981)1326-1332.

82 P. D. Ewing and J. G. Williams, "Thickness and Moisture Content Effect in the Fracture Toughness of Scots Pine", *Journal of Materials Science*, 14 (1979) 2959-2966.

83 W. G. Ferguson and M. N. Sargisson, "Fracture Toughness of Comsteel En 25", *Engineering Fracture Mechanics*, 5 (1973) 499-508.

84 S. J. Garwood, "Measurement of Crack Growth Resistance of A533B Wide Plate Tests", *Fracture Mechanics: Twelfth Conference, ASTM STP 700*, (1980) 271-295.

85 G. Green and J. F. Knott, "On Effects of Thickness on Ductile Crack Growth in Mild Steel", *Journal of the Mechanics and Physics of Solids*, 23 (1975) 167-183.

86 G. H. Hilton, "Evaluation of Ti-6A1-4V for Specification Requirements", *Fraction Prevention and Control*, American Society for Metals, (1974) 181-197.

87 K. Ikeda and H. Kihara, "Brittle Fracture Strength of Welded Structures", *Proceedings of the Second International Conference on Fracture*, Brighton, U.K. (1969) 851-867.

88 G. R. Irwin, "Fracture", *Encyclopedia of Physics*, 6 (1958) 551-590.

89 G. R. Irwin, "Effects of Size and Shape on Fracture of Solids", *Properties of Crystalline Solids, ASTM STP 283*, (1960) 118-128.

90 G. R. Irwin, "Fracture Mode Transition for a Crack Traversing a Plate", *Journal of Basic Engineering, Transactions of the ASME*, June (1960) 417-423.

91 G. R. Irwin, "Fracture Mechanics", *Structural Mechanics*, Pergamon Press, New York, (1960) 557-594.

92 F. A. Johnson and J. C. Radon, "Mechanical and Metallurgical Aspects of Fracture Behaviour of an Al-Alloy", *International Journal of Fracture Mechanics*, 8 (1972) 21-36.

93 F. A. Johnson, and J. C. Radon, "Fracture Energy and Crack Tunnelling", *Journal of Testing and Evaluation*, 4 (1976) 209-217.

94 M. F. Kaplan, "Crack Propagation and the Fracture of Concrete", *Journal of the American Concrete Institute*, 58 (1961) 591-609.

95 J. G. Kaufman and H. Y. Hunsicker, "Fracture Toughnes Testing at Alcoa Research Laboratories", *Fracture Toughness Testing and its Applications, ASTM STP 381* (1965) 290-308.

96 J. G. Kaufman, R. L. Moore, and P. E. Schilling, "Fracture Toughness of Structural Aluminum Alloys", *Engineering Fracture Mechanics*, 2 (1971) 197-210.

97 M. O. Lai and W. G. Ferguson, "The Inadequacy of the Plane-Strain Fracture Toughness Test Requirements", *Engineering Fracture Mechanics*, 13 (1980) 285-292.

98 H. W. Liu, "Thickness Effects on Fracture Criteria", *Fracture Mechanics of Ductile and Tough Materials and Its Applications to Energy Related Structures*, (1981) 189-198.

99 H. W. Liu and C. Y. Yang, "Strip Yielding Model and Fracture Toughnesses of Thin and Tough Plates", *Fracture Mechanics in Engineering Application* (1979) 55-66.

100 Y. W. Mai, A. G. Atkins, and R. M. Caddell, "Determination of Valid *R*-Curves for Materials with Large Fracture Toughness to Yield Strength Ratios", *International Journal of Fracture*, 12 (1976) 391-407.

101 G. Marci, J. Eschweiler, and T. Fett, "Fracture Toughness of 7075-T7351 Aluminum Plates", *Proceedings of the Fourth European Conference on Fracture*, Leoben, Austria, 1 (1982) 118-126.

102 R. H. Marloff, M. M. Leven, T. N. Ringler and R. L. Johnson, "Photoelastic Determination of Stress-intensity Factors", *Experimental Mechanics*, December (1971) 529-539.

103 M. J. May, "British Experience with Plane Strain Fracture Toughness (K_{Ic}) Testing", *Review of Developments in Plane Strain Fracture Toughness Testing, ASTM STP 463*, (1970) 41-62.

104 I. Milne and G. G. Chell, "Effect of Size on the *J* Fracture Criterion", *Elastic-Plastic Fracture, ASTM STP 668* (1979) 358-377.

105 T. Nakazawa, S. Suzuki, T. Sunami, and Y. Sogo, "Application of High-Purity Ferritic Stainless Steel Plates to Welded Structures", *Toughness of Ferritic Stainless Steels, ASTM STP 706*, (1980) 99-122.

106 F. G. Nelson, J. G. Kaufman, and E. T. Wanderer, "Tear Tests of 5083 Plate and of 5183 Welds in 5083 Plate and Extrusions", *Advances in Cryogenic Engineering*, 15 (1970) 91-101.

107 J. O. Outwater, M. C. Murphy, R. G. Kumble, and J. T. Berry, "Double Torsion Technique as a Universal Fracture Toughness Test Method", *Fracture Toughness and Slow-Stable Cracking, ASTM STP 559*, (1974)127-138.

108 B. K. Parida, "Crack Edge Instability–A Criterion for Safe Crack Propagation Limit in Thin Sheets", *Proceedings of the Third Colloquium on Fracture* (1980) 307-314.

109 J. S. Pascover, M. Hill, and S. J. Matas, "The Application of Fracture Toughness Testing to the Development of a Family of Alloy Steels", *Fracture Toughness Testing, ASTM STP 381*, (1965) 310-323.

110 V. K. Pujari, I. Finnie, and F. E. Hauser, "A Moving-load Controlled-displacement Fracture-toughness Testing Machine", *Experimental Mechanics*, June (1981) 234-239.

111 D. Rhodes, L. E. Culver, and J. C. Radon, "The Influence of Fracture Mode Transition on the Compliance of Thin Section Fracture Specimens", *Proceedings of the Third Colloquium on Fracture*, London, U.K., (1980) 287-296.

112 J. C. Ritter, "A Modified Thickness Criterion for Fracture Toughness Testing", *Engineering Fracture Mechanics*, 9 (1977) 529-540.

113 R. Roberts, G. V. Krishna, and G. R. Irwin, "Fracture Behavior of Bridge Steels", *Flaw Growth and Fracture, ASTM STP 631* (1977) 267-284.

114 S. T. Rolfe and S. R. Novak, "Slow-Bend K_{Ic} Testing of Medium-Strength High-Toughness Steels", *Review of Developments in Plane Strain Fracture Toughness Testing, ASTM STP 463* (1970)124-159.

115 A. Savadori, C. Marega, and E. Marchetti, "Morphology and Molecular Weight in the High Speed Fracture Mechanics of Polypropylene", *Proceedings of International Conference Analytical Experimental Fracture Mechanics*, Rome, Italy (1980) 931-941.

116 F. R. Schwartzberg, "A Review of Cryogenic Fracture Toughness Behavior", *Advances in Cryogenic Engineering*, 12 (1967) 458-472.

117 W. Seidl, "Specimen Size Effects on the Determination of K_{Ic}-Values in the Range of Elastic-Plastic Material Behavior", *Engineering Fracture Mechanics*, 12 (1979) 581-597.

118 Special ASTM Committee on Fracture Testing of High-Strength Sheet Materials (Pt. 1). *ASTM Bulletin*, January (1960) 29-40.

119 Special ASTM Committee on Fracture Testing of High-Strength Sheet Materials (Pt. 2), *ASTM Bulletin*, February (1960)18-28.

120 J. E. Srawley, "Plane Strain Fracture Toughness Tests on Two-inch-thick Maraging Steel Plate at Various Strength Levels", *Proceedings of the Second International Conference on Fracture*, Brighton, U.K., (1969) 131-146.

121 J. L. Swedlow, *The Thickness Effect and Plastic Flow in Cracked Plates*, Aerospace Research Laboratories, OH, ARL 65-216 (1965)1-139.

122 M. G. Vassilaros, J. A Joyce, and J. P. Gudas, "Effects of Specimen Geometry on the J_I-R Curve for ASTM A533B Steel", *Fracture Mechanics: Twelfth Conference, ASTM STP 700* (1980) 251-270.

123 K. Wallin, "The Size Effect in K_{Ic} Results", *Engineering Fracture Mechanics*, 22 (1985) 149-163.

124 V. Weiss and S. Yukawa, "Critical Appraisal of Fracture Mechanics", *Fracture Toughness Testing and Its Application, ASTM STP 381* (1965) 1-29.

125 R. H. Weitzmann and I. Finnie, "Further Studies of Crack Propagation Using the Controlled Crack Propagation Approach", *Fracture Toughness and Slow-Stable Cracking, ASTM STP-559* (1974) 111-126.

126 E. T. Wessel, W. G. Clark, Jr., and W. H. Pryle, "Fracture Mechanics Technology Applied to Heavy Section Steel Structures", *Proceedings of the Second International Conference on Fracture*, Brighton, U.K., (1969) 825-850.

127 A. D. Wilson, "The Influence of Inclusions on the Toughness and Fatigue Properties of A516-70 Steel", *Journal of Engineering Materials and Technology, Transactions of the ASME*, 101 (1979) 265-274.

128 T. M. Wright and W. C. Hayes, "Fracture Mechanics Parameters for Compact Bone – Effects of Density and Specimen Thickness", *Journal of Biomechanics*, 10 (1977) 419-430.

129 O. F. Yap, Y. W. Mai, and B. Cotterell, "Thickness Effect on Fracture in High Impact Polystyrene", *Journal of Materials Science*, 18 (1983) 657-668.

130 H. Yoshimura, H. Masumoto, T. Inoue, "Properties of Low-Carbon 25Mn-5Cr-1Ni Austenitic Steel for Cryogenic Use", *Advances in Cryogenic Engineering*, 28 (1982) 115-125.

131 J. M. Barsom, E. J. Imhof and S. T. Rolfe, "Fatigue-crack Propagation in High Yeild-Strength Steels", *Engineering Fracture Mechanics*, 2 (1971) 301-317.

132 W. R. Brose and N. E. Dowling, "Size Effects on the Fatigue Crack Growth Rate of Type 304 Stainless Steel", *Elastic-Plastic Fracture, ASTM STP 668* (1979) 720-735.

133 W. G. Clark, Jr., "Effect of Temperature and Section Size on Fatigue Crack Growth in Pressure Vessel Steel", *Journal of Materials*, 6 (1971) 134-149.

134 W. G. Clark, Jr. and H. E. Trout, Jr., "Influence of Temperature and Section Size on Fatigue Crack Growth Behavior in Ni-Mo-V Alloy Steel", *Engineering Fracture Mechanics*, 2 (1970) 107-123.

135 N. E. Dowling, "Fatigue-Crack Growth Rate Testing at High Stress Intensities", *Flaw Growth and Fracture, ASTM STP 631* (1977) 139-158.

136 L. A. James, "Specimen Size Considerations in Fatigue Crack Growth Rate Testing", *Fatigue Crack Growth Measurement and Data Analysis, ASTM STP 738* (1981) 45-57.

137 Metals Handbook, 9th ed., Vol 4 Heat Treating, *American Society for Metals*, Metals Park OH. (1981) 14-27.

138 1985 Annual Book of ASTM Standards, Vol. 03.01, *American Society for Testing and Materials*, Philadelphia, (1985) 130-151

139 J. F. Knott, *Fundamentals of Fracture Mechanics*, Butterworths, London (1981).

140 1985 Annual Book of ASTM Standards, Vol. 03.01, *American Society for Testing and Materials*, Philadelphia, (1985) 1-56.

141 C. W. MacGregor, "The True Stress-Strain Tension Test- Its Role in Modern Materials Testing, Pt 1", *Journal of the Franklin Instute*, 238 (1944) 111-135.

142 W. Weibull, "A Statistical Theory of the Strength of Materials", *Proceedings of the Royal Swedish Institute for Engineering Research*, 151 (1939) 5-45.

143 1985 Annual Book of ASTM Standards, Vol. 03.01, *American Society for Testing and Materials*, Philadelphia, (1985) 739-749.

144 C. G. Annis, R. M. Wallace and D. L. Sims, "A Interpolative Model for Elevated Temperature Fatigue Crack Propagation", *AFML - TR-76-176 Part 1* (1976).

145 H. S. Carslaw and J. C. Jaeger, *Conduction of Heat in Solids, 2nd Ed.*, Oxford at the Clarendon Press, 1959.

APPENDIX A. TABLES OF THICKNESS DATA

The thickness data gleaned from the references is herein presented in a format to complement other local work [1.7]. The following tables present data grouped with respect to material tested, i.e., steels, aluminum alloys, other metals, and non-metals. In each of these, the table format is the same and begins with the contributor's surname and reference number. Below this is a generic identification of the specific material reported, e.g., for steel, 4340; aluminum, 2024-T635; for other metals, T_i6A-6V-2Sn, etc.. These entries are followed by an indication of specimen used according to the following abbreviations: CCP...center cracked panel, CTS...compact tension specimen, RCT...round compact tension, RDS...rotating disk specimen, SEN...single-edge notch, WOL...wedge opening loading, 3PB...three-point bend, 4PB...four-point bend.

The number in parentheses following one of the above abbreviations indicates the total number of specimens reported. If a further number follows, it represents the testing temperature: no further such number indicates tests performed at room temperature. The fourth column in the table represents the normalizing or representative thickness, B_0. The next column is the thickness scaling factor for the specimens reported, λ_B. The fourth column is the ratio of reported critical strength to that at a thickness of B_0, i.e., σ_i^*/σ_0^*. The final column classifies the response in accordance with: b...brittle, b-d...brittle ductile, and d...ductile.

Table A.1 Sources and data for steels

Source, material, specimen type (# tested)	Temp.	B_o [in.]	λ_B	$\frac{\sigma_i}{\sigma_0}$	Classification
Andrews et al. [9], A469,CD[2-6]		1.0	0.38	0.47	d
			0.77	0.85	d
			1.54	1.59	d
		1.35	0.55	0.98	b-d
			1.11	1.00	b
			2.22	1.01	b
Bandyopadhyay et al. [10], 0.22 C, 0.87 Mn, 0.07 Si, 0.02 S, & 0.02P; 3PB [18]		0.045	2.73	1.19	d
		5.00	1.32	d	
			8.70	1.26	d
			22.12	1.28	d
		0.071	1.67	1.11	d
			3.17	1.27	d
			5.71	1.29	d
		0.151	0.75	0.97	d
			1.46	1.04	d
			6.49	1.37	d
		0.215	1.11	1.02	d
			1.82	1.11	d
		0.245	0.47	0.96	d
			0.96	1.00	d
			1.55	0.98	d
			4.32	1.16	d
Banerjee [11], ASTM 516-Gr70, CT		0.5	0.20	0.92	d
			0.39	0.95	b-d
			0.67	0.98	b-d
			1.0	1.0	b-d
			2.0	1.05	b-d
Barnby and Al-Daimalani [12], BS1956A C-1Cr, 3PB (10 - 30)		0.44	0.89	0.98	d
			1.33	1.05	d
			1.78	1.03	d
			2.22	1.00	b-d
			2.67	0.98	b-d
			3.56	1.06	b-d
BS1348E $^1/_2$Cr-$^1/_2$Mo-$^1/_2$V,3PB (10 -30)		0.44	0.89	1.03	b-d
			1.33	0.98	b-d

Table A.1 (con't)

Source, material, specimen	Temp.	B_o	λ_B	$\frac{\sigma_i}{\sigma_0^*}$	Class.
			1.78	0.95	b-d
			2.22	1.07	b-d
BS1458A		0.44	0.89	1.07	d
$1^1/_2$Mn-Ni-Gr-Mo, 3PB (10 -30)			1.33	0.88	d
			1.78	0.86	b-d
			2.22	0.87	b-d
			2.67	0.91	b-d
BS1458B		0.44	1.33	1.06	d
$1^1/_2$Ni-Cr-Mo, 3PB (15 & 25)			2.22	1.18	b-d
Barnby and Al-Daimalani [13],		0.44	0.89	1.02	d
BS1760B, 3PB (25 & 30)			1.33	0.98	d
			1.78	1.05	d
			2.22	1.05	b-d
			2.67	1.10	b-d
BS1456A		0.44	2.22	1.34	d
$1^1/_2$Mn, 3PB (10 & 30)			2.67	1.42	d
Batte et al [15],		0.2	2.00	1.27	d
1%Cr Mo V 1P, SEN			4.00	1.57	d
Brown and Sprawley [18],		0.25	0.40	1.07	b-d
Maraging steel,4PB			0.60	1.04	b-d
			1.00	1.02	b-d
			1.40	0.97	b-d
Maraging steel,SEC		0.5	0.20	1.13	b
			0.50	1.02	b
			1.00	1.00	b
Maraging steel,CCP		0.5	0.20	1.12	b
			0.50	1.01	b
			1.00	1.00	b
Maraging steel,4PB		0.1	1.00	1.00	d
			5.00	0.88	d
Maraging steel, SEC		0.5	0.20	1.00	b
			0.50	1.03	b
			0.80	1.02	b
Maraging steel, CCP		0.5	0.20	1.10	b
			0.50	1.10	b
			0.80	1.04	b
Maraging steel, 4PB		0.11	0.91	0.98	b

Table A.1 (con't)

Source, material, specimen	Temp.	B_0	λ_B	$\frac{\sigma_i}{\sigma_0^*}$	Class.
			3.64	0.97	b
Chell and Worthington [20], Ducol W30A, CTS, (8)		1.37	0.36	0.99	d
			0.73	0.95	d
		1.09	1.01	d	
	1.45	0.90	d		
		1.00	0.50	1.13	d
			1.00	1.00	d
			1.50	1.06	d
			2.00	0.92	d
Elsender et al. [21], 1%CrMoV1P, SENT		0.45	8.69	1.20	d
			16.95	1.27	d
Fukakura [23], 0.15 C, 0.01 Si, 0.71 Mn, 0.01 P, 0.02 S; 4PB	-148^0F	0.10	0.80	1.09	d
			2.00	0.77	d
			4.00	0.70	b-d
			6.00	0.71	b-d
			8.00	0.78	d
			12.00	0.72	d
Griffis [25],* HY-80, 3PB		0.125	1.91	1.08	d
			0.97	1.0	d
			0.49	0.86	d
Hollstein et al. [27], St E 460, SEN		0.29	2.72	1.02	d
			5.44	1.04	d
		0.47	0.86	0.99	d
			1.72	1.03	d
			3.43	1.08	d
		0.63	0.62	0.98	d
			1.23	1.01	d
			2.46	1.01	d
		0.79	0.50	1.03	d
			0.99	1.00	d
			1.98	0.97	d
		0.94	0.42	0.96	d
			0.84	0.99	d
Huang and Gelles [28], HT-9, CT		0.25	0.39	1.00	d
			1.19	1.00	d
			1.87	1.03	d
Jones and Brown [32],		0.135	0.37	0.94	b-d

Table A.1 (con't)

Source, material, specimen	Temp.	B_o	λ_B	$\frac{\sigma_i}{\sigma_0^*}$	Class.
E4340, 3PB			0.74	1.02	b-d
			0.93	1.00	b-d
			1.48	1.02	b-d
			1.93	1.02	b-d
			2.20	1.01	b
			3.70	1.02	b
		0.25	0.17	0.99	b
			0.30	1.03	b
			0.48	1.02	b
			0.89	0.97	b
			1.04	1.01	b
			1.20	1.00	b
			1.64	1.00	b
			2.16	0.98	b
			2.40	0.98	b
			3.92	0.99	b
		0.55	0.11	1.08	b
			0.20	1.05	b
			0.38	1.05	b
			0.49	1.05	b
			0.55	1.06	b
			0.60	1.07	b
			0.95	1.02	b
			1.00	1.00	b
			1.89	0.98	b
Kaiser and Hagedorn [33], 30CrNiMo8, CT	~32°F	1.00	0.20	0.76	b-d
			0.40	0.89	b-d
			0.80	0.97	b-d
Ke and Liu [36], HY-80, SEN		0.8	0.16	0.97	d
			0.31	0.88	d
			0.66	0.91	d
			1.18	1.04	d
Knott [38], 2%C Steel, 4PB	-140°F		1.5	0.94	d
			3.0	0.84	d
			4.5	0.71	d
			6.0	0.70	d
			12.0	0.68	d
	-85°F		1.20	0.90	d
			2.4	0.60	d
			3.6	0.48	d
			4.8	0.53	d
			6.0	0.57	d

Table A.1 (con't)

Source, material, specimen	Temp.	B_o	λ_B	$\frac{\sigma_i}{\sigma_0^*}$	Class.
	-184°F		1.2	1.0	d
			2.4	1.02	d
			3.6	0.60	d
			4.8	0.57	d
			6.0	0.96	d
Mowbray et al. [42], A-302B, 3PB	~-50°F	0.04	5.0	1.23	d
			10.0	1.40	d
	-100°F	0.04	5.0	1.05	d
			10.0	1.11	d
	-150°F	0.04	5.0	0.84	d
			10.0	0.73	d
Ni-Mo-V, SEN	-100°F	0.164	0.12	1.75	d
			0.76	1.09	d
	-320°F	0.164	0.12	1.7	d
			0.76	1.22	d
Munz and Keller [43], 35Ni-CR-Mo-16	-184°F	0.6	0.20	0.93	b-d
			0.40	1.02	b-d
			0.67	1.02	b-d
			1.00	1.00	b-d
			1.67	1.02	b-d
	-166°F	0.6	0.20	0.88	b-d
			1.00	1.00	b-d
			1.67	1.00	b-d
	-148°F	0.6	0.20	0.72	b-d
			0.40	0.76	b-d
			0.67	0.96	b-d
			1.00	1.00	b-d
	-130°F	0.6	0.20	0.72	b-d
			0.40	1.05	b-d
			0.66	0.95	b-d
			1.00	1.00	b-d
			1.66	1.28	b-d
	-112°F	0.6	0.66	1.06	b-d
			1.00	1.00	b-d
			1.66	1.25	b-d
Neale [44],		1.03	1.89	0.98	b-d

Table A.1 (con't)

Source, material, specimen	Temp.	B_o	λ_B	$\frac{\sigma_i}{\sigma_0^*}$	Class.
1Cr-Mo-V, CT $a_{ave.}$ ±4%			0.95	1.02	b-d
			0.48	1.65	d
			0.25	2.04	d
			0.12	2.46	d
Poulose et al. [47],		0.75	0.31	2.04	d
4340 (L-T)			0.67	1.08	d
			1.00	0.90	d
			1.00	1.00	d
			1.33	0.35	d
			1.67	0.32	d
Putatunda and Banerjee [48],		0.27	0.16	0.94	d
CT			0.29	0.87	d
			0.60	0.95	d
Riccardella and Swedlow [51],		0.25	1.00	1.00	d
A533 Grade B Class 1, CCDogbone			2.00	1.06	d
			4.00	1.10	d
Rolfe and Novak [52],		1.50	0.20	1.16	b-d
18 Ni Maraging, 3 PB			0.33	1.06	b
			0.66	1.06	b
			1.33	0.96	b
			2.00	0.97	b
		1.00	0.20	1.05	b-d
			0.30	1.04	b-d
			0.50	0.99	b
			0.75	0.98	b
			1.00	1.00	b-d
			2.00	0.95	b
Shannon et al. [54],		0.125	2.00	0.99	d
D6aC, DEN			4.00	0.99	d
		0.25	1.00	1.00	d
			2.00	0.87	d
			4.00	0.89	d
		0.50	1.00	1.00	b-d
			2.00	0.97	b-d
18Ni (250)		0.125	2.00	1.04	d
			4.00	1.08	d
		0.25	1.00	1.00	d
			2.00	0.80	d
			4.00	0.81	d

Table A.1 (con't)

Source, material, specimen	Temp.	B_0	λ_B	$\frac{\sigma_i}{\sigma_0^*}$	Class.
		0.50	1.00	1.00	d
			2.00	0.77	b-d
300M		0.125	2.00	1.01	b-d
			4.00	1.02	d
		0.25	1.00	1.00	b
			2.00	1.03	b
			4.00	1.08	b
		0.50	1.00	1.00	b
			2.00	1.05	b
Sliney, Jr. [55], 5% Cr-Mo-V, DEN	200°F	0.075	0.53	0.92	d
			0.80	0.97	d
			1.07	0.98	d
			1.33	0.92	d
	76°F	0.075	0.27	1.96	d
			0.53	1.60	d
			0.80	1.67	d
			1.07	1.63	d
			1.33	1.54	d
	-40°F	0.075	0.27	1.25	d
			0.53	1.15	d
			1.07	1.07	d
			1.33	1.05	d
	-65°F	0.075	0.27	2.14	d
			0.53	1.64	d
			0.08	2.10	d
	-100°F	0.075	0.27	3.66	d
			0.53	2.64	d
CCP	76°F	0.857	0.05	3.06	d
			0.14	2.1	d
			0.19	2.08	d
			0.25	2.09	d
Srawley and Beachem [57], G8 steel, CCP	80°F	0.25	0.52	0.93	d
			0.40	0.89	d
			0.32	0.84	d
			0.24	1.02	d
			0.16	1.55	d
			0.08	1.32	d

Table A.1 (con't)

Source, material, specimen	Temp.	B_0	λ_B	$\frac{\sigma_i}{\sigma_0^*}$	Class.
68 Steel, CCP	0°F	0.25	0.40	1.31	d
			0.20	1.61	d
	-100°F	0.25	0.40	1.07	d
			0.20	1.13	d
	-200°F	0.25	0.40	0.96	b-d
			0.20	0.94	b-d
	-280°F	0.25	0.40	1.48	b
			0.20	1.99	b
W2, CCP	+300°F	0.25	0.40	0.99	d
			0.32	0.99	d
			0.24	0.97	d
			0.16	0.94	d
			0.08	0.93	d
	80°F	0.25	0.40	1.09	d
			0.32	1.11	d
			0.24	1.09	d
			0.16	1.07	d
			0.08	1.01	d
	-280°F	0.25	0.40	1.23	b
			0.32	1.29	b
			0.24	1.28	b
			0.16	1.40	b
			0.08	1.38	b
Steigerwald [58], H-11, CCP		0.175	0.09	1.50	b-d
			0.15	1.39	b-d
			0.21	1.16	b
			0.30	0.83	b
			0.55	1.03	b
Steigerwald and Hanna [59], AM 355 SST, CCP		0.175	0.01	0.20	d
			0.01	0.18	d
			0.02	0.17	b-d
			0.02	0.05	b-d
			0.03	0.16	b-d
Sullivan and Stoop [60], 4130, CCP		0.97	0.03	0.52	d
			0.06	0.58	d
		1.68	0.02	0.27	b-d
			0.03	0.32	d

Table A.1 (con't)

Source, material, specimen	Temp.	B_0	λ_B	$\frac{\sigma_i}{\sigma_0^*}$	Class.
			0.04	0.35	d
		1.24	0.03	1.38	d
			0.10	1.23	d
		0.80	0.06	2.22	d
			0.11	1.86	d
		0.93	0.07	0.45	d
			0.13	0.55	d
		1.64	0.02	4.56	d
			0.03	4.48	b-d
			0.05	3.60	b-d
D6A, CCP		1.03	0.09	0.03	b
			0.18	0.02	b
			0.24	0.04	b
		0.53	0.18	0.26	b
			0.36	0.23	b
			0.46	0.33	b
Taira and Tanaka [62], Cr-Mo-V, CT	392°F	0.39	0.2	1.95	b-d
			0.5	1.30	b
			1.0	1.00	b
			2.0	0.77	b
	1112°F	0.39	0.2	0.98	d
			0.5	1.10	d
			1.0	1.00	d
			2.0	0.82	b-d
Winne and Wundt [65], Ni-Mo-V, RDS		1.32	1.52	0.88	b-d
			4.56	0.64	b
Ni-Mo-V (0.27 Mo), RDS		1.32	4.56	0.71	d
			2.66	0.81	d
Cr-Mo-V		1.50	4.00	0.97	b
			1.33	0.99	b
Yukawa [66], Alloy steel		0.4	0.31	2.08	d
			0.94	1.00	b
			1.56	1.00	b
			2.50	0.94	b
			10.00	0.92	b

Table A.2 Sources and data for aluminum

Source, material, specimen type (# tested)	Temp.	B_0 [in.]	λ_B	$\frac{\sigma_i}{\sigma_0^*}$	Classification
Bathias [14], 2618-T6, CCP		0.65	0.06	2.50	d
			0.12	2.93	d
			0.18	2.84	d
			0.24	3.08	d
			0.30	2.59	d
2618-T651, CCP		0.65	0.06	3.72	d
			0.12	3.41	d
			0.18	3.37	d
			0.24	3.14	d
			0.30	3.75	d
			0.36	3.57	d
			0.48	3.16	d
			0.61	2.17	b-d
7075-T6, CCP		0.65	0.06	1.59	d
			0.12	1.96	d
			0.18	2.06	d
			0.24	1.97	d
			0.30	2.03	d
			0.39	1.74	b-d
7075-T651, CCP		0.65	0.06	1.33	d
			0.12	1.43	d
			0.18	1.36	d
			0.24	1.27	b-d
			0.30	1.25	b-d
			0.36	1.21	b-d
			0.48	1.15	b-d
			0.61	1.10	b-d
7075-T7351, CCP		0.65	0.06	0.80	d
			0.12	0.90	d
			0.18	0.89	d
			0.24	0.86	d
			0.30	0.90	d
			0.36	0.67	b-d
			0.48	0.84	d
			0.61	0.89	d
2024-T4, CCP		0.65	0.06	1.10	d
			0.18	1.31	d
			0.24	1.25	d
			0.30	1.29	d
			0.36	1.24	d

Table A.2 (con't)

Source, material, specimen	Temp.	B_0	λ_B	$\frac{\sigma_i}{\sigma_0^*}$	Class.
2024-T351, CCP		0.65	0.06	1.06	d
			0.12	1.17	d
			0.18	1.18	d
			0.24	1.18	d
			0.30	1.24	d
			0.36	1.16	d
			0.48	1.09	d
			0.61	1.06	d
Frediani [22], 2219-T851, CCP		0.22	0.45	1.01	d
			0.72	1.00	d
		0.36	0.13	0.88	d
			0.27	0.89	d
			0.43	0.93	d
		0.43	0.11	1.04	d
			0.23	1.03	d
		0.57	0.08	0.91	d
			0.17	0.89	d
			0.28	0.92	d
		0.64	0.07	0.95	d
			0.15	1.00	d
			0.25	1.00	d
		0.78	0.06	0.78	d
			0.13	0.78	d
			0.20	0.82	d
Grewal and Weiss [24], 2024-T351, SEN		0.25	1.00	1.00	d
			0.50	1.07	d
			0.25	1.15	d
		0.25	1.00	1.00	d
			0.50	0.91	d
			0.25	0.82	d
Heyer and McCabe [26], 7075-T6, CCP		0.38	0.17	1.55	d
			0.08	1.84	d
Hudson and Lewis [29], 2219-T851, Not stated		1.50	1.00	1.02	b
			0.83	1.63	d
			0.58	1.98	d
			0.33	2.06	d
			0.17	2.37	d

Table A.2 (con't)

Source, material, specimen	Temp.	B_o	λ_B	$\frac{\sigma_i}{\sigma_0}$	Class.
Irwin et al. [30],		0.33	2.28	1.24	b
7075-T6 , 3PB			1.12	1.03	b
Kaufman [34],		0.25	0.25	1.72	d
7079-T6, -T651, DEN			0.50	1.61	d
			1.00	1.00	d
7075-T6, -T651, DEN		0.25	0.25	1.50	d
			0.13	1.40	d
			1.0	1.00	d
Kaufman [35],		0.125	1.0	1.00	d
7178-T7651, SEN			1.6	0.99	d
			2.0	0.97	d
			3.0	0.94	d
			4.0	0.93	d
		0.75	0.27	1.16	b
			0.50	1.10	b
			0.66	1.08	b
			1.00	1.00	b
			1.33	0.97	b
Liebowitz et al. [39],		0.75	0.66	0.83	b
2048-T851, CT			0.92	0.98	b
			1.18	1.06	b
			1.44	0.81	b
			1.97	0.88	b
Morozov [41],		0.6	0.40	1.14	d
Di6, CCP			0.87	1.02	d
			1.67	0.98	d
			2.60	1.16	d
Pook [46],		0.5	2.00	0.99	b-d
4% Cu alloy to BS 2L65, 3PB			1.00	1.50	b-d
Poulose et al. [47],		0.75	0.08	5.16	d
7075-T651, CT			0.17	4.60	d
			0.33	2.40	b
			0.50	1.67	b
			0.67	1.35	b
2124-T851, CT		0.75	0.67	1.32	b
			1.00	1.00	b
			1.33	1.40	b
			1.67	0.76	b
			2.00	0.82	b

Table A.2 (con't)

Source, material, specimen	Temp.	B_0	λ_B	$\frac{\sigma_i}{\sigma_0^*}$	Class.
2048-T851, (L-T), CT		0.75	0.67	1.20	b-d
			0.93	1.04	b-d
			1.20	0.90	b-d
			1.47	0.66	b
			2.00	0.64	b
2048-T851, (T-L), CT		0.75	0.67	1.44	b
			0.83	1.16	b
			1.00	1.00	b
			1.33	0.91	b
			1.50	0.87	b
2048-T351, (LT), CT		0.75	0.67	1.39	d
			1.00	1.00	d
			1.33	0.83	b-d
			1.67	0.95	b-d
			2.00	0.95	b-d
		1.00	0.50	1.30	d
			0.75	1.48	d
			1.00	1.00	d
			1.25	1.07	d
			1.50	0.95	d
		0.50	1.00	1.00	b-d
			1.50	0.94	b-d
			2.00	0.91	b-d
Read and Reed [49], 2219-T87, CT	-460°F	0.6	0.25	1.34	b-d
			0.47	1.11	b
			0.93	1.01	b
Shannon et al. [54], 2419, DEN		0.125	2.0	0.93	d
			4.0	0.87	d
		0.25	1.0	1.00	d
			2.0	0.85	d
			4.0	0.77	d
		0.50	1.0	1.00	d
			2.0	0.85	d
7075-T7351		0.125	2.0	0.96	d
			4.0	0.93	d
		0.25	1.0	1.00	d
			2.0	0.83	d
			4.0	0.62	d

Table A.2 (con't)

Source, material, specimen	Temp.	B_0	λ_B	$\frac{\sigma_i}{\sigma_0^*}$	Class.
		0.50	1.0	1.00	d
			2.0	0.64	d
Sullivan and Stoop [60],		0.61	0.07	0.80	b-d
7178-T6, CCP			0.10	1.00	d
			0.15	0.88	b-d
			0.21	0.90	b-d
7079-T6, CCP		0.87	0.04	0.68	d
			0.07	0.78	d
			0.29	0.89	d
2014-T6, CCP		0.82	0.05	1.31	d
			0.11	1.31	d
			0.31	1.16	d
2219-T87, CCP		0.96	0.03	0.81	d
			0.09	0.86	d
7075-T6, CCP		0.69	0.09	1.89	d
			0.44	1.24	b-d
7475-T61, CCP		0.75	0.14	1.03	d
			0.25	1.02	d
		1.04	0.10	0.47	d
			0.18	0.39	d
			0.24	0.45	d
		1.4	0.05	4.77	d
			0.14	2.79	d
		1.66	0.04	1.32	d
			0.15	1.18	d
		1.15	0.09	1.76	d
			0.22	1.45	d
Sullivan et al. [61],		0.5	0.06	2.38	d
7075-T6, CCP (ELOX precrack)			0.13	2.85	d
			0.18	3.04	d
			0.20	2.93	d
			0.25	2.58	b-d
			0.40	2.77	d
			0.50	2.14	b-d
7075-T6, CCP (fatigue pre-cracked)	0.5	0.06	1.13	d	

Table A.2 (con't)

Source, material, specimen	Temp.	B_o	λ_B	$\frac{\sigma_i}{\sigma_0^*}$	Class.
			0.13	1.01	d
			0.18	1.32	d
			0.20	1.01	b-d
			0.25	0.95	b-d
			0.40	0.93	b-d
			0.50	0.95	b-d
7075-T6, CCP		1.0	0.06	2.14	d
			0.13	2.20	d
			0.19	2.44	d
			0.20	1.95	b-d
			0.25	1.73	b-d
			0.40	1.79	b-d
			0.50	1.55	b
7079-T6, CCP (ELOX crack)		0.5	0.07	0.64	d
			0.12	0.73	d
			0.20	1.02	d
			0.27	0.71	d
			0.50	0.83	d
7079-T6, CCP (fatigue crack)		0.5	0.07	0.69	d
			0.12	0.81	d
			0.20	1.06	d
			0.27	0.77	d
			0.50	0.87	d
2014-T6, CCP (ELOX crack)		0.5	0.08	1.58	d
			0.13	1.52	d
			0.18	1.58	d
			0.25	1.94	d
			0.50	1.40	d
2014-T6, CCP (fatigue crack)		0.5	0.08	1.53	d
			0.13	1.34	d
			0.18	1.38	d
			0.25	1.60	d
			0.50	1.26	d
Zinkham [67],		0.25	0.51	0.91	b-d
7075-T6 (L), CCP			0.71	0.95	b-d
		0.76	0.16	0.86	b
			0.25	0.97	b
			0.33	0.97	b
			0.41	0.97	b
(T), CCP		0.25	0.50	1.02	b-d
			0.75	1.01	b-d

Table A.2 (con't)

Source, material, specimen	Temp.	B_0	λ_B	$\frac{\sigma_i}{\sigma_0^*}$	Class.
		0.76	0.16	1.19	b
			0.25	1.29	b
			0.33	1.34	b
			0.42	1.26	b

Table A.3 Sources and data for other metals

Source, material, specimen type (# tested)	Temp.	B_0 [in.]	λ_B	$\frac{\sigma_i}{\sigma_0^*}$	Classification
Johnson [31], Ti-6Al-4V, CTS		1.22	0.04	1.58	b-d
			0.32	1.18	b
Jones and Brown [32], Ti-6Al-6V-2Sn		0.25	0.08	1.59	b-d
			0.24	1.27	b
			0.52	0.96	b
			1.00	1.00	b
			2.04	1.01	b
Poulose et al. [47], Ti-6Al-4V		0.75	0.17	1.13	d
			0.33	1.09	b-d
			0.67	1.03	b-d
			1.00	1.00	b-d
			1.33	0.86	b-d
Repko et al. [50], DEN	76°F	0.075	1.73	1.10	d
			0.84	1.08	d
			0.33	1.34	d
			0.24	1.54	d
			0.13	1.76	d
		0.075	0.24	0.86	b-d
			0.33	1.67	d
			0.84	1.06	d
			1.73	0.83	b-d
		0.225	0.08	1.04	b-d
			0.11	2.35	b-d
			0.28	1.41	b-d
			0.58	1.16	b
		0.075	0.24	1.00	d
			0.31	1.00	d
			0.84	1.00	d
			1.73	1.00	d
		0.225	0.08	1.00	d
			0.10	1.00	d
			0.28	1.00	d
			0.58	1.00	d
	-110°F	0.075	0.24	0.96	d
			0.31	1.00	d
			0.84	1.05	d

Table A.3 (con't)

Source, material, specimen	Temp.	B_0	λ_B	$\frac{\sigma_i}{\sigma_0^*}$	Class.
			1.73	0.86	d
	-320°F	0.075	0.24	0.79	d
			0.31	0.79	d
			0.84	1.06	d
			1.73	0.83	d
Shannon et al. [54], Ti-6A1-4V		0.125	2.0	0.87	d
			4.0	0.76	d
		0.25	1.0	1.00	d
			2.0	0.82	d
			4.0	0.63	d
		0.50	1.0	1.00	d
			2.0	0.65	d
Ti-8M_0-8V		0.25	1.0	1.00	b-d
			2.0	0.96	d
			4.0	0.95	d
		0.50	1.0	1.00	b
			2.0	0.98	b
Srawley and Beachem [57], Ti-13V-11Cr-3Al,CCP	80°F	0.25	0.52	1.47	b-d
			0.40	1.70	b-d
			0.32	1.70	b-d
			0.24	1.92	b-d
			0.16	1.88	b-d
			0.08	2.00	b-d
Sullivan and Stoop [60], Ti-4Al-3Mo-1V, CCP		0.55	0.08	14.5	b
			0.11	15.6	b
			0.16	17.9	b
			0.23	10.1	b
Ti-16V-2.5Al, CCP		0.645	0.06	1.53	b
			0.18	1.30	b
Ti-13V-11A-3Al, CCP		0.53	0.08	3.77	b
			0.12	4.22	b
			0.17	3.33	b
Williams [63], Ti-4Al-3Mo-1V, CT		0.088	2.86	0.83	b-d
			1.48	1.00	d

Table A.4 Sources and data for non-metals

Source, material, specimen type (# tested)	Temp.	B_o [in.]	λ_B	$\frac{\sigma_i}{\sigma_0^*}$	Classification
Behiri and Bonfield [16], Bone, bovine (long axis), CT		0.18	0.11	0.98	d
			0.22	1.00	d
			0.33	1.00	d
			0.44	1.00	d
Birch et al. [17], uPVC, 4PB	72°F	0.05	4.8	0.94	d
			9.6	0.91	d
			14.4	0.86	d
			18.4	1.02	d
		0.10	1.2	1.03	d
			2.4	1.13	d
			4.8	1.09	d
			7.2	1.16	d
			9.2	1.06	d
		0.15	0.8	0.94	d
			1.6	1.15	d
			3.2	1.04	d
			4.8	1.04	d
			6.13	1.07	d
		0.2	0.6	0.97	d
			1.2	1.01	d
			2.4	1.05	d
			3.6	1.03	d
			4.6	0.98	d
		0.25	0.48	0.92	d
			0.96	1.00	d
			1.92	0.94	d
			2.88	0.88	d
			3.68	0.93	d
Chan and Williams [19], Hi-dens. polythylene, 3PB		0.072	2.73	0.55	d
			5.46	0.37	d
			10.92	0.46	d
		0.14	1.43	0.94	d
			2.86	0.83	d
			5.71	0.94	d
		0.21	0.95	1.020	d
			1.90	0.78	d

Table A.4 (con't)

Source, material, specimen	Temp.	B_0	λ_B	$\frac{\sigma_i}{\sigma_0^*}$	Class.
			3.80	0.87	d
Kinloch and Gledhill [37], Nitrocellulose/nitro-glycerine propellant, CT	68°F	1.0	0.4	0.89	b
			2.0	1.09	b
	32°F	1.0	0.4	1.07	b
			2.0	0.95	b
	-4°F	1.0	0.4	1.23	b
			2.0	0.85	b
	-76°F	1.0	0.4	1.42	b
			2.0	0.80	b
Mindess and Nadeau [40], Mortar, 3PB		1.0	3.98	0.86	b
			8.03	0.80	b
			12.0	0.82	b
			16.0	0.84	b
			20.0	0.83	b
Concrete, 3PB		1.0	3.54	1.08	b
			8.03	1.13	b
			12.0	1.10	b
			16.0	1.18	b
			20.0	1.07	b
Petrie et. al. [45], Polycarbon. sheet(Lexan 9030), CT		0.5	0.40	1.13	b
			1.0	1.06	b
Schmidt and Lutz [53], Westerly granite		1.97	0.27	0.99	b-d
			0.5[illegible]	1.04	b-d
			1.04	0.99	b-d
			1.53	1.00	b-d
			2.04	1.02	b-d
Smith and Chowdary [56], Slip-cast fused silica, 3PB		0.238	1.14	1.05	b
			1.72	1.23	b
			1.92	0.97	b
			2.11	1.15	b
Williams and Ewing [64], Polymethylmethacrylate, SEN		0.055	2.25	0.87	b-d
			4.50	0.78	b-d
		0.105	1.19	0.96	b-d
			2.38	0.83	b-d
		0.15	0.83	0.96	b-d
			1.66	1.10	b-d

APPENDIX B. COOLING TIME CALCULATIONS

In this appendix we present a method of estimating how long the test specimens need to sit in liquid nitrogen (LN_2) in order to reach equilibrium. We start by developing a simplified physical model, then formally state the problem to be solved. After this we present a solution leading to a means of obtaining the times. We close by discussing the reliability of these estimates.

The geometry of the specimens is as shown earlier in Figure 3.1. Computing the hold time in LN_2 for the center to reach the same temperature as the surface is a problem of heat conduction in a solid. Such problems have been extensively handled by Carslaw and Jaeger [145]. Although there is no solution for this exact geometry in [145], we can make use of Carslaw and Jaeger by setting up the problem at hand in a simplified model. The simple model chosen to represent the specimens is a finite length hollow cylinder, Figure B-1.

This model is sized so that the inside radius, r_i, is one half of the machined notch width, as indicated by the dashed lines in Figure B.1. The outside radius, r_o, is selected so that the model shares the same length ahead of the uncracked ligament. The thickness, B, is taken to be the same as for the fracture specimen. All surfaces are awash with LN_2, and therefore we assume that they come to LN_2 temperature virtually immediately.† The left half of Figure B.1 is the region of greatest interest in the specimen and specifically we are concerned with the temperature along the $\theta = 0$ line, the probable trajectory of the fracture.

---

† This assumption was confirmed with surface thermocuple measurements.

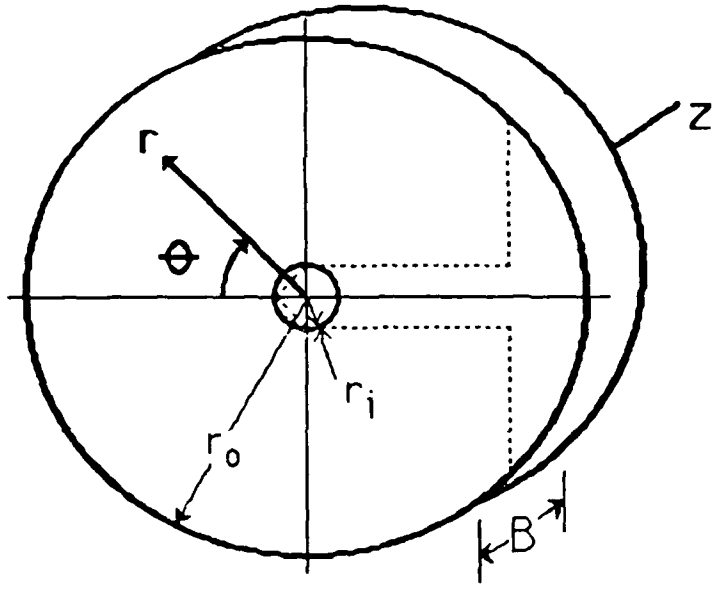

Figure B.1. Model geometry used for thermal calculations

The general problem statement for this model geometry proceeds as follows. We seek to find the time for a piece of 1045 steel, in the geometry shown in Figure B.1, to reach equilibrium when taken from room temperature and immersed in a bath of liquid nitrogen. In order to determine this equilibrium time, t_e, we need to find the axisymmetric temperature distribution, $T = T(r,z,t)$ for all time t (>0) throughout $\boldsymbol{R}$, where $\boldsymbol{R}$ is the region defined by

$$\boldsymbol{R} \equiv \{(r,\theta,z) \mid r_i < r < r_o,\ -\pi < \theta < \pi,\ -B/2 < z < B/2\},$$

and r, θ, z are cylindrical polar coordinates, (Figure B.1).

The temperature distribution is to satisfy:

$$\nabla^2 T = \frac{1}{K}\frac{\partial T}{\partial t} \qquad (B.1)$$

on R for t>0, where $\nabla^2 = \frac{\partial^2}{\partial r^2} + \frac{1}{r}\frac{\partial}{\partial r} + \frac{\partial^2}{\partial z^2}$ in the Laplacian operator and K is the conductivity; and the initial and boundary conditions,

$$T = T_r \text{ at } t = o \text{ on } \boldsymbol{R}$$

$$T = T_I \text{ on } r = r_i, r_o \ (-\pi < \theta < \pi, -B/2 < z < B/2, 0 < t) \text{ and} \qquad (B.2)$$

$$T = T_I \text{ on } z = \pm B/2 \ (-\pi < \theta < \pi, r_i < r < r_o, 0 < t)$$

The solution to the above problem can be found in essence in Carslaw and Jaeger [145], Sections 7.10 and 8.4, and is:

$$T = T_I + (T_r - T_I) X \Psi \qquad (B.3)$$

where $X \equiv \pi \sum_{n=1}^{\infty} \exp(-K\alpha_n^2 t) \frac{J_0(\alpha_n r_i)\, U_0(\alpha_n r)}{J_0(\alpha_n r_i) + J_0(\alpha_n r_o)}$ and

$$\Psi \equiv \frac{4}{\pi} \sum_{n=0}^{\infty} \frac{(-1)^n}{2n+1} \exp\left(\frac{-K(2n+1)^2\pi^2 t}{b^2}\right) \cos\left(\frac{(2n+1)\pi z}{B}\right)$$

Here $J_0(\alpha_n r)$ is a Bessel function of the first kind, order zero, $Y_0(\alpha_n r)$ is a Bessel function of the second kind, order zero, $U_0(\alpha_n r)$ is the associated Wronskien ($U_0(\alpha_n r) = J_0(\alpha_n r)Y_0(\alpha_n r_o) - J_0(\alpha_n r_o)Y_0(\alpha_n r)$) and α_n are the eigen values of the problem, these eigen values are obtained from the roots of $U_0(\alpha_n r_i) = 0$.

Since the time we seek, that to reach equilibrium, is long ($t_e >> 1$), the series solutions of both X and Ψ are dominated by the initial terms. This domination is the result of the presence of exponentials raised to negative powers that depend upon time. In the Ψ expression the influence of the terms drops off quickly since the power of the exponent changes by a factor of nine in the first step, and more in the subsequent ones. Therefore we only apply the first term. However the behavior of the X expression depends on how α_n varies, and that variation is not

obvious. For simplicity at this time, we deal with the first term in the X series and comment on this choice subsequently.

Since T is a function of position, we must identify the last point to reach the desired temperature. With respect to the z dimension, from symmetry, we can see that this occurs on the z=0 plane. However, it is not so obvious in the r direction. To get the r position which has the highest temperature, we take the derivative of (B.3), with respect to r, and equate it to zero to obtain an r , r_m, which maximizes the temperature, *i.e.* , we set $\frac{\partial T}{\partial r} = 0 \Rightarrow \frac{\partial X}{\partial r} = 0 \Rightarrow \frac{\partial U_0(\alpha r)}{\partial r} = 0.$

Combining the identity for U_0 and the expressions $\partial J_0(\alpha_n r)/\partial r = -\alpha_n J_1(\alpha_n r)$ and $\partial Y_0(\alpha_n r)/\partial r = -\alpha_n Y_1(\alpha_n r)$ then yields:

$$J_0(\alpha_n r_o)Y_1(\alpha_n r_m) - J_1(\alpha_n r_m)Y_0(\alpha_n r_o) = 0. \qquad (B.4)$$

Equation (B.3) can be solved numerically to provide r_m. Using the location of the last point to cool in conjunction with truncating the exponential series in t then gives (for t>>1), for the maximum temperature, T_m,

$$T_m = T_1 + 4(T_r - T_1)\left[\frac{J_0(\alpha_1 r_i)\, U_0(\alpha_1 r_m)}{J_0(\alpha_1 r_i) + J_0(\alpha_1 r_0)}\right] \exp(-Kt_e(\alpha_1^n + (\frac{\pi}{B})^2)) \qquad (B.5)$$

This can be rearranged to give:

$$t_e = \left[\frac{-1}{K(\alpha^2 + (\frac{\pi}{B})^2)}\right] \ln\left[\frac{T_m - T_1}{4(T_r - T_1)}\left(\frac{J_0(\alpha_1 r_i)\, U_0(\alpha_1 r_m)}{J_0(\alpha_1 r_i) + J_0(\alpha_1 r_0)}\right)\right] \qquad (B.6)$$

We are now in a position to discuss a method of obtaining t_e using the above equations. The first step is to find the eigen values for X, the most important being the first, namely α_1. Using α_1 in (B.4), we find a value for r_m within the region, then having α_1 and r_m, we evaluate $U_0(\alpha_1 r_m)$. Our final step is to substitute the known quantities into (B.6) and solve for the time. We do this using as a definition of equilibrium here, T_m within 1% of T_l which is the temperature at $t = \infty$.

Since there are eleven combinations of B's and r's, a table of values is in order and is shown in Table B.1.

We note in Table B.1 that if the equilibrium requirement is made more stringent so that it requires uniformity to within say 0.1 percent, the cooling times are increased by a factor of about 1.4. We also comment upon the values of properties used to compute K, namely k the thermal conductivity, ρ the density, and C the specific heat. These values are commonly given in references at room temperature or higher. All these properties vary with temperature, although k and ρ do so to a small extent. However, C can change and usually gets smaller, thus increasing the value of K. As seen in (B.6), t is inversely proportional to K, so that an increase in K will shorten t_e. Finally we remark on the use of only the first term in the X series. After computing the series with and without the second through fourth terms for the two inch diameter specimens, we find that for t_e= 100 seconds the value of the X expression is reduced at r_m by about 10%. However when t_e exceeds 500 seconds, the reduction is less than 0.5%. Hence there is little effect. The additional terms reduce the value of X, and hence t_e, because $U_0(\alpha_n r_n)$ is negative for n= 2 and 3. Thus the times calculated from (B.6) can reasonably be expected to be used as upper bounds.

TABLE B.1 Specimen cooling times

Specimen size	B (in)	r_o (in)	r_i (in)	α_1	r_m (in)	t_e (min)
1x 3/8	0.375	0.421	0.031	7.5787	0.182	6.4
1x 3/4	0.75	"	"	"	"	10.9
2x 3/32	0.093	0.842	0.062	3.7894	0.363	0.7
2 x3/16	0.186	"	"	"	"	2.7
2x3/8	0.375	"	"	"	"	9.6
2x3/4	0.75	"	"	"	"	25.5
2x3/2	1.5	"	"	"	"	43.4
2x2 1/4	2.25	"	"	"	"	49.9
4x3/8	0.375	1.684	0.124	1.8947	0.727	11.1
4x3/4	0.75	"	"	"	"	38.5
4x3/2	1.5	"	"	"	"	102.0

In arriving at the above the following parameter values, which are independent of size, are used:

$\alpha_1 r_o = 3.191$ $\alpha r_i = 0.2349$ $U_o(\alpha_1 r_m) = 0.2833$

$$\frac{J_0(\alpha_1 r_i)\, U_o(\alpha_1 r_m)}{J_0(\alpha_1 r_i) + J_0(\alpha_1 r_o)} = 0.4180$$

$(T - T_I)/(T_r - T_I) = 0.39/390.04\ ^\circ R/^\circ R = 0.001$

$K = k/(\rho C) = 1.52 \times 10^{-4}\ in^2/sec\ (^\circ R/^\circ R)$

APPENDIX C. EXPERIMENTAL DETAILS

Here we present details of the experiments described above. The appendix consists of three tables which give the information for preliminary and extended monotonic experiments, and cyclic loading experiments.

TABLE C.1 Details of preliminary experimental series.

Specimen I.D.	B (in)	a (in)	W (in)	P^* (Klb)	σ_n^* (Ksi)
1 45 1	2.98	0.71	1.48	8.41	34.78
1 45 2A†	2.98	0.75	1.48	7.53	35.38
1 45 3A	2.99	0.75	1.48	7.77	35.86
1 45 4A	2.99	0.76	1.48	7.99	38.16
1.3 45 1A	2.25	0.83	1.48	5.49	43.10
1.3 45 2A	2.25	0.80	1.48	5.89	43.26
2 45 1	1.50	0.82	1.48	3.59	40.66
2 45 2	1.50	0.83	1.48	3.80	45.49
2 45 3A	1.50	0.89	1.48	3.46	49.72
2 45 4A	1.50	0.87	1.48	3.45	46.85
4 45 1	0.75	0.89	1.50	2.38	65.24
4 45 2A	0.75	0.82	1.50	2.65	58.59
8 45 1	0.37	0.78	1.50	2.00	76.45
8 45 2	0.37	0.85	1.49	1.43	70.17
8 45 3A	0.37	0.80	1.50	1.39	57.50
16 45 1	0.19	0.82	1.50	0.72	63.66
16 45 2A	0.19	0.80	1.50	0.78	65.47
32 45 1	0.09	0.81	1.49	0.38	66.20
32 45 2A	0.09	0.80	1.49	0.41	70.35
64 45 1	0.05	0.80	1.48	0.20	68.86
64 45 2	0.05	0.80	1.48	0.18	63.88
64 45 3A	0.05	0.80	1.48	0.20	70.52
64 45 4A	0.05	0.80	1.48	0.18	64.17
64 45 5A	0.05	0.80	1.48	0.17	60.50
64 45 7A	0.04	0.80	1.48	0.18	65.32
64 45 8A	0.04	0.80	1.48	0.18	65.06
64 45 9A	0.04	0.80	1.48	0.17	63.04

† A indicates testing after heat treating.

TABLE C.2 Details of extended experimental series.

Specimen ID	B (in)	a (in)	W (in)	P^* (Klb)	σ_n^* (Ksi)	f	NN Vol†
4 2 1	1.50	1.62	2.96	5.35	29.95	1.0	
4 2 2	1.50	1.64	2.94	5.46	31.48	1.0	
4 2 3	1.50	1.59	2.97	5.74	30.31	0.0	
				ADJ AVE	30.72	2.0	1.0
4 4 1	0.75	1.64	2.97	2.77	32.13	1.0	
4 4 2	0.75	1.59	2.96	2.92	31.32	0.0	
4 4 3	0.75	1.60	2.96	2.87	31.17	0.3	
				ADJ AVE	31.91	1.3	0.5
4 8 1	0.37	1.63	2.97	1.63	36.93	1.0	
4 8 2	0.37	1.63	2.97	1.51	33.61	1.0	
4 8 3	0.37	1.76	2.97	1.19	32.39	0.46	
4 8 4	0.37	1.59	2.97	1.57	33.23	0.5	
4 8 5	0.37	1.60	2.97	1.59	34.46	0.5	
4 8 6	0.37	1.63	2.97	1.50	33.68	1.0	
4 8 7	0.37	1.67	2.97	1.39	33.45	1.0	
				ADJ AVE	34.14	5.46	0.25
2 1.3 1	2.25	0.84	1.48	4.53	37.62	0.5	
2 1.3 2	2.25	0.78	1.48	5.41	36.11	0.17	
2 1.3 3	2.25	0.81	1.48	4.86	36.22	1.0	
				ADJ AVE	36.63	1.67	0.37

† Normalized nominal volume

TABLE C.2 (con't)

Specimen ID	B (in)	a (in)	W (in)	P* (Klb)	σ_n* (Ksi)	f	NN Vol†
2 2 1	1.5	0.70	1.48	4.81	38.69	0.0	
2 2 2	1.5	0.87	1.48	2.92	40.10	1.0	
2 2 3	1.5	0.70	1.48	4.48	35.82	1 0	
2 2 4	1.5	1.01	1.48	2.40	58.67	0.0	
2 2 5	1.5	0.96	1.48	2.84	55.01	0.0	
2 2 6	1.5	0.90	1.48	2.86	43.26	0.86	
2 2 7	1.5	1.02	1.48	3.05	77.00	0.0	
				ADJ AVE	39.55	2.86	0.25
2 4 1	0.75	0.79	1.48	1.72	35.81	0.0	
2 4 2	0.75	0.84	1.48	1.61	40.30	0.5	
2 4 3	0.75	0.79	1.48	1.84	38.92	0.5	
				ADJ AVE	39.61	1.0	0.12
2 8 1	0.37	0.79	1.48	0.92	38.75	0.0	
2 8 2	0.37	0.85	1.48	0.79	40.56	1.0	
2 8 3	0.37	0.81	1.48	0.86	38.28	1.0	
2 8 4	0.37	0.80	1.48	0.87	38.23	1.0	
2 8 5	0.37	0.79	1.48	0.90	38.73	0.0	
2 8 6	0.37	0.8	1.48	0.99	43.29	1.0	
2 8 7	0.37	0.80	1.48	0.90	38.95	1.0	
				ADJ AVE	39.86	5.0	0.06
2 16 1	0.19	0.82	1.48	0.49	45.87	1.0	
2 16 2	0.19	0.81	1.48	0.46	41.00	1.0	
2 16 3	0.19	0.82	1.48	0.47	44.51	1.0	
				ADJ AVE	43.79	3.0	0.03
2 32 1	0.09	0.81	1.48	0.23	42.13	0.3	
2 32 2	0.09	0.83	1.48	0.23	44.52	1.0	
2 32 3	0.09	0.81	1.48	0.23	42.30	0.3	
2 32 4	0.09	0.81	1.48	0.23	42.64	0.3	

TABLE C.2 (con't)

Specimen ID	B (in)	a (in)	W (in)	P* (Klb)	σ_n* (Ksi)	f	NN Vol†
2 32 5	0.09	0.81	1.48	0.23	42.57	0.3	
2 32 6	0.09	0.81	1.48	0.24	43.83	0.3	
2 32 7	0.09	0.81	1.48	0.24	43.88	0.3	
				ADJ AVE	43.47	2.8	0.015
1 4 1	0.75	0.41	0.74	1.51	69.86	1.0	
1 4 2	0.75	0.42	0.74	1.07	51.62	1.0	
1 4 3	0.74	0.37	0.74	1.46	51.92	0.16	
1 4 4	0.74	0.41	0.75	1.16	53.03	1.0	
				ADJ AVE	57.85	3.16	0.03
1 81	0.37	0.41	0.74	0.55	49.85	1.0	
1 8 2	0.37	0.35	0.74	0.77	47.99	0.0	
1 8 4	0.37	0.43	0.74	0.59	63.32	0.21	
1 8 5	0.37	0.43	0.74	0.49	51.56	0.5	
1 8 6	0.37	0.52	0.74	0.45	111.	0.0	
1 8 7	0.37	0.38	0.74	0.83	65.96	0.5	
				ADJ AVE	55.16	2.21	0.016

TABLE C.3 Details of cyclic experiments.

DATA CODE #	LOAD (lb) MAX/MIN	CYCLES TO FAILURE	INITIAL CRACK (in)	FINAL CRACK (in) Lf/Rt	LAST MEAS. CRACK (IN) Lf/Rt	TOTAL a_c (in)
L-6	4000/400	27000	0.917	.776/.714	.700/.457	2.45
L-3	"	26100	0.916	.790/.742	.584/.447	2.49
L-8	"	26800	0.961	.764/.763	.474/.631	2.49
S-10	250/25	76900	0.243	.182/.155	.189/.134	0.587
S-6	"	85500	0.246	.193/.171	.151/.171	0.610
S-5	"	85100	0.245	.192/.167	.185/.146	0.604
S-3	"	74700	0.245	N/A	.082/.078	N/A
S-9	"	77500	0.246	.175/.166	.184/.157	0.596
S-7	"	81600	0.246	.147/.183	.175/.160	0.604
L-10	4000/400	28200	0.959	.782/.647	.608/.377	2.39
L-11	"	28100	0.963	.701/.788	.461/.682	2.45
L-9	"	28100	0.959	.690/.790	.517/.755	2.44